

A 2MASS All-Sky View of the Sagittarius Dwarf Galaxy: VII. Kinematics of the Main Body of the Sagittarius dSph

Peter M. Frinchaboy^{1,2,3,4}, Steven R. Majewski⁵, Ricardo R. Muñoz^{6,7}, David R. Law⁸,
Ewa L. Lokas⁹, William E. Kunkel¹⁰, Richard J. Patterson⁵, and Kathryn V. Johnston¹¹

p.frinchaboy@tcu.edu, srm4n@vigrinia.edu, rmunoz@das.uchile.cl,
drlaw@di.utoronto.ca, lokas@camk.edu.pl, kunkel@lcoeps1@lco.cl,
rjp0i@vigrinia.edu, kvj@astro.columbia.edu

ABSTRACT

We have assembled a large-area spectroscopic survey of giant stars in the Sagittarius (Sgr) dwarf galaxy core. Using medium resolution ($R \sim 15,000$), multifiber spectroscopy we have measured velocities of these stars, which extend up to 12 degrees from the galaxy's center (3.7 core radii or 0.4 times the King limiting radius). From these high quality spectra we identify 1310 Sgr members out of 2296 stars surveyed distributed across 24 different fields across the Sgr core. Additional slit spectra were obtained of stars bridging from the Sgr core to its trailing tail. Our systematic, large area sample shows no evidence for significant rotation, a result at odds with the ~ 20 km s⁻¹ rotation required as an explanation for the bifurcation seen in the Sgr tidal stream; the observed small (≤ 4 km s⁻¹) velocity trend along primarily the major axis

¹Department of Physics & Astronomy, Texas Christian University, TCU Box 298840, Fort Worth, TX 76129

²National Science Foundation Astronomy and Astrophysics Postdoctoral Fellow, University of Wisconsin–Madison, Department of Astronomy, 5534 Sterling Hall, 475 N. Charter Street, Madison, WI 53706.

³Visiting Astronomer, Cerro Tololo Inter-American Observatory, National Optical Astronomy Observatory, which is operated by the Association of Universities for Research in Astronomy, Inc. (AURA) under cooperative agreement with the National Science Foundation.

⁴Any opinions, findings, and conclusions or recommendations expressed in this material are those of the author(s) and do not necessarily reflect the views of the National Science Foundation.

⁵Department of Astronomy, University of Virginia, P.O. Box 400325, Charlottesville, VA 22904-4325, USA

⁶Astronomy Department, Yale University, P.O. Box 208101, New Haven, CT 06520-8101 USA

⁷Departamento de Astronomía, Universidad de Chile, Casilla 36-D, Santiago, Chile (current address)

⁸Dunlap Institute for Astronomy & Astrophysics, University of Toronto, 50 St. George Street, Toronto M5S 3H4, Ontario, Canada

⁹Nicolaus Copernicus Astronomical Center, Bartycka 18, 00-716 Warsaw, Poland

¹⁰Las Campanas Observatory, Casilla 601, La Serena, Chile

¹¹Department of Astronomy, Columbia University, New York, NY 10027, USA

is consistent with models of the projected motion of an extended body on the sky with no need for intrinsic rotation. The Sgr core is found to have a flat velocity dispersion (except for a kinematically colder center point) across its surveyed extent and into its tidal tails, a property that matches the velocity dispersion profiles measured for other Milky Way dwarf spheroidal (dSph) galaxies. We comment on the possible significance of this observed kinematical similarity for the dynamical state of the other classical Milky Way dSphs in light of the fact that Sgr is clearly a strongly tidally disrupted system.

Subject headings: Local Group – galaxies: individual (Sgr dSph) – galaxies: kinematics and dynamics

1. INTRODUCTION

The Sagittarius (Sgr) dwarf galaxy is a satellite of the Milky Way (MW) with an apparent dwarf spheroidal (dSph) morphology that is, however, distinct in at least two ways. First, the relative proximity of Sgr to the Sun ($d \approx 24$ kpc) makes its brightest stars quite accessible to study with even relatively modest aperture telescopes. Thus, Sgr is open to much more straightforward and extensive examination than its much more distant, counterpart MW satellites making Sgr, in principle, a highly approachable, local laboratory for dSph galaxies. Second, Sgr represents the most certain and vivid example of a satellite enduring tidal disruption by the MW, with the highest known surface brightness tidal tails among MW dSph satellites. Indeed, not only does no other MW dSph have anywhere near as obvious tidal debris, whether other dSphs are showing any evidence of visible mass loss is still debated for most MW satellites. For this reason, Sgr is often relegated to a “special case” category among MW satellites and investigators of the properties of “classical dSphs” often avoid Sgr because of an uncertainty and wariness of how it fits into the larger dSph context. Obviously prudence dictates care in such matters, but the potential advantages of a much more accessible test laboratory for dSph dynamics makes it worth understanding whether the second of the above two Sgr properties (tidal disruption) truly nullifies the usefulness of the first (proximity) in terms of adopting Sgr as a valid prototype for other dSph satellites.

An early analysis of the internal dynamics of Sgr was provided by Ibata et al. (1997). This impressively assembled early sample of radial velocities numbered some 410 stars using the CTIO/ARGUS and AAT/AUTOFIB spectrographs, and it remains the only fully published wide-spread detailed analysis of the dynamical properties of the Sgr galaxy main body. While the area covered provides some strength to look at the larger Sgr main body, the limitation of most fields being along the main axis limits further analysis, as does the poor velocity precision of the AAT data ($\epsilon_{RV} \sim 12$ km s⁻¹). However, many analyses of the dynamics and M/L of this system specifically make use of the single dispersion (~ 11 km s⁻¹) derived for Ibata et al.’s database of 114 stars located at the nucleated (perhaps unrepresentative) center.

Recently, a first analysis of a new AAT data set was presented by, Peñarrubia et al. (2011), based on 1805 Sgr members by RV in 6 fields along the major axis and one side of the minor axis of Sgr reaching to $\pm 4^\circ$ along the major axis. This data analysis and modeling focuses primarily on whether rotation is found in Sgr.

An improved kinematical analysis of the Sgr inner core and attempting to isolate it chemically and kinematically from M54 was conducted by Bellazzini et al. (2008). They analyzed 1152 VLT/FLAMES and Keck/DEIMOS spectra using RVs and CaT metallicities determinations to isolate the Sgr core population from that of M54. While this provides an excellent analysis of the central core of Sgr ($\sigma_v = 9.6 \pm 0.4 \text{ km s}^{-1}$), the limited area, all within $9'$ of core, provides just one data point compared to the larger main body of Sgr.

Of course, understanding the Sgr system — among the nearest known examples of a minor merger — is sufficient cause for systematic exploration of its core, whether or not it can be considered a suitable representative of the dSph morphological class in general. Some recent evidence makes a compelling case that the primary difference between Sgr and other MW satellites may be principally in its life phase within what may be a universal evolutionary course for dwarf galaxies. In general, the star formation histories of dwarf galaxies in the local universe are similar for most of cosmic time, regardless of their present morphological type, with the latter mostly a function of variations in the influence of external mechanisms (like ram pressure stripping or tidal effects) within the past Gyr or so and that give rise to a strong morphology-density relationship (Skillman et al. 2003; Grebel 2004; Weisz et al. 2011). According to models by Mayer et al. (2001), tidal stirring via close passages around large host galaxies can transform star forming, gas-rich, dwarf irregular (dIrr) systems with small rotating disks into classical, moribund, gas-depleted, pressure-supported dSphs. The mechanism driving such a metamorphosis is the formation and decline of a central bar, incited by the dynamical interaction of the satellite with the gravitational potential of the host, particularly at pericenter passages. Certainly it is clear that at least some of the present “classical” MW dSphs (e.g., Carina, Leo I), though now devoid of gas, were forming stars in the not too distant past (the past few Gyrs; Smecker-Hane et al. 2009; Gallart et al. 2007) — just like Sgr (Siegel et al. 2007). Interestingly, Carina and Leo I may be the two classical MW dSphs apart from Sgr with the strongest evidence for tidal disruption (Carina: Irwin & Hatzidimitriou 1995; Kuhn, Smith, & Hawley 1996; Majewski et al. 2000, 2004; Muñoz, Majewski, & Johnston 2008, Leo I: Sohn et al. 2007; Mateo et al. 2008).

Ironically, despite Sgr’s proximity, less is known about the distribution of properties of stars across the Sgr core than for other satellites of the MW, for a variety of potential reasons — e.g., because of (1) the tendency of observers to avoid it on grounds that it is perceived to be unusual, as mentioned above, (2) the fact that Sgr has only been relatively recently discovered (Ibata et al. 1994), as well as, probably most importantly, (3) its intrinsic size at its distance from the Sun means that Sgr spans a large angle on the sky. Even with large field of view, multifiber spectroscopy it is simply difficult to cover the enormous size of the Sgr core (with a semi-major axis length of almost 30 degrees). Nevertheless, some basic knowledge about the Sgr core is, of course, in place.

Ibata et al. (1994, 1995) made the first maps showing the extended and elongated nature of the Sgr core and determined that it was comparable in size and luminosity to the largest of the MW dSph satellites, the Fornax system. These authors also showed that, like Fornax, the Sgr system has its own retinue of globular clusters, including M54, a large globular cluster that is either the very heart, or *at* the very heart, of the dSph (see discussion by Bellazzini et al. 2008; Monaco et al. 2005; but also cf. Siegel et al. 2011). Other globular clusters in the Galactic halo farther from the Sgr core may also be debris from the original satellite (see review by Law & Majewski 2010b).

Majewski et al. (2003; hereafter PAPER I) assembled the first all-sky view of the Sgr dwarf galaxy core along with its tidal tails by identifying constituent M giant stars within the final release Two Micron All-Sky Survey (2MASS; Skrutskie et al. 2006) point source catalog. M giants, which are copious in the relatively metal rich ($[\text{Fe}/\text{H}]$ as high as -0.4 ; Layden & Sarajedini 2000) Sgr populations, are separable from M dwarfs with J, H, K photometry (Bessell & Brett 1988), and in any case the former well outnumber the latter to 2MASS magnitude limits (e.g., $K_s \sim 13 - 14$). The 2MASS M giant sample, which is more robust to the differential reddening effects that have made optical studies of Sgr core difficult, yielded the first “clean” view of the entire main Sgr body. From the distribution of the large population of M giants, the morphology of the Sgr core could be more accurately fit, and Majewski et al. showed that it could be described by a King profile but with, at the largest radii, a break in the King profile due to the presence of its tidal tails. Apart from the fact that Sgr shows a small density cusp at its very center, which may or may not (see Monaco et al. 2005) be due to the density enhancement provided by the superposition of M54, the overall King+power law break profile of Sgr looks identical to those previously observed in other “classical” Galactic dSphs (see Fig. 13 below); however, the source of these profile breaks in other dSph systems have been debated as due either to prodigious tidal mass loss or as bound populations expected for the high inferred M/L in these systems (e.g., Munoz et al. 2006, 2008; Sohn et al. 2007; Koch et al. 2007; McConnachie, Peñarrubia, & Navarro 2007). It is commonly suggested (e.g., Kroupa 1997; Kleyana et al. 1999) that discrimination of these two models should be possible from the radial velocity (RV) dispersion trend with radius. Sgr represents the closest, most accessible dSph in the class of those exhibiting King+break profiles, but it is also the one example where the break is from *certain* tidal disruption. Thus it provides a Rosetta Stone by which the dynamical markers of this process may be empirically established.

In the present paper we undertake the first large, wide-field *and* high resolution ($R \sim 15,000$) spectroscopic survey to sample across the larger area encompassing the core body of the Sgr system. With this survey, we explore the velocity distribution of 2MASS-selected K and M giant stars across the face of this core, from its very center out to the trailing tidal tail and along the major, minor and other symmetry axes of the system. Thus, with this survey we provide kinematical information for Sgr that is comparable in extent to datasets existing for other Milky Way dSphs. This enables us to put Sgr in a dynamical context with these other systems, and provide a baseline for comparison to a dSph known to be undergoing severe tidal disruption. Our study focuses on two primary observables to provide this context: (1) Within the distribution of radial velocities (§3) we look for

signatures of rotation and show that Sgr, like other dSphs, has no significant rotation signature (§4). (2) The velocity dispersion profile of Sgr is shown to be more or less flat, which is the same trend found in all other dSphs (§5). Thus, in these two properties, Sgr is found not to be unusual compared to other dSphs, despite its current state of enduring extreme mass loss (see, e.g., PAPER I; Chou et al. 2007). We comment on the potential significance of this apparent “normality” of Sgr as a dSph system for the potential state of other dSph systems in §6.2.

2. SPECTROSCOPIC SURVEY OF THE SGR CORE

2.1. Survey Coverage and Observations

The present survey systematically samples the core of the Sgr dSph galaxy with target fields selected primarily along the major and minor axes. Additional pointings along diagonal directions give greater leverage in mapping the kinematical and chemical distributions of the dwarf. Fields were selected to explore the major axis at $\sim 2^\circ$ intervals, the minor axis at $\sim 1^\circ$ intervals, and the diagonals at $+2^\circ$ and $+4^\circ$ radial separations (Fig. 1). The precise field centers were allowed to shift by a few arcmin to maximize the number of observable targets, as described below.

The potential target stars were selected to be late type giants as identified in dereddened $(J - K_s, K_s)$ color-magnitude diagrams from the 2MASS catalog. The 2MASS photometry was dereddened using the Schlegel et al. (1998) maps, with their $E(B - V)$ values converted to $E(J - K_s)$ and $A(K_s)$ using the relations given in PAPER I. The maximum inferred mean reddening in any field was $\langle E(J - K_s) \rangle = 0.224$ in Minor+05. Stars that may belong to the Sgr red giant branch (RGB) were selected using the following color-magnitude region:

- $9 < K_{s,0} < 14$
- $K_{s,0} > -8.8(J - K_s)_0 + 19.1$
- $K_{s,0} < -8.8(J - K_s)_0 + 21.6$

This selection was made to isolate the Sgr RGB in the Sgr core (e.g., field Major+00) while minimizing the contamination from Galactic stars, as shown in Figure 2, though distance and metallicity variations can cause the mean RGB color and magnitude to shift which was not accounted for in this study.

Spectroscopic data were obtained using the Hydra spectrograph on the Blanco 4-m telescope at CTIO on the nights of 19–22 July 2003 and 1–7 August 2003 under mostly clear skies with good seeing (estimated $1.2''$). Data were obtained using 132 fibers that are simultaneously dispersed onto a 2048×4096 pixel CCD (SITe400mm) using the 380 grating ($1200 \text{ lines mm}^{-1}$) and with the fiber ends viewed by the spectrograph through a $100\mu\text{m}$ slit plate to improve the resolution to 0.68 \AA per resolution element ($R \sim 15,000$). The spectral range covered was 7740–8740 \AA and we

typically exposed for 60 minutes per field to obtain spectra with signal-to-noise ratios (S/N) of 5 for stars at the faintest limit of $K_s \sim 14.0$.

Potential Sgr stars were weighted by magnitude and input to the `hydra_assign` program that is used to design fiber configurations for the Hydra multi-object spectrograph on the Blanco 4-m telescope at the Cerro Tololo Inter-American Observatory (CTIO). The `hydra_assign` parameters were set to maximize the number of Sgr candidate stars selected, and this was done by testing the total weights for assigned fibers at each field centering for a spatial search grid of $15' \times 15'$ with $1'$ steps centered on the nominal field center. The centers of the actually observed fields using this optimization plan are found in Table 1 and shown in Figure 1.

Along with our target fields, we also observed a selection of radial velocity standard stars. For each of these RV standards, we obtained multiple observations, where each “observation” entails sending the light of the calibrator down 2-12 different fibers with slightly differing exposure lengths to be able to measure the trend of velocity precision with data quality.

3. RADIAL VELOCITIES AND MEMBERSHIP ANALYSIS

3.1. Measuring the Radial Velocities

Radial velocities were determined using IRAF `fxcor`, which cross-correlates stellar templates with the object stars based on the methodology of Tonry & Davis (1979). For this study, the stellar templates were high- S/N RV standard stars. The region used in the cross-correlation was 8220–8680 Å. A full discussion of the data reduction and calibration to the IAU standard RV system can be found in Frinchaboy & Majewski (2008); the present data were obtained on the same nights using the same “red” RV standards.

Only stars with S/N of 5 or better were included in the RV analysis. However, spectral template mismatches also produce poor results, so an additional culling based on the Tonry-Davis ratio ($TDR > 3$) was also employed. The TDR selection is used over a S/N one because the TDR statistic also accounts for the effects of mismatches (e.g., due to temperature/chemistry differences) of a target star’s photosphere with that of the velocity template; the TDR therefore provides a better correlation to the measured velocity errors. We determined our velocity uncertainties as fully described in Frinchaboy & Majewski (2008) and adopting the method of Vogt et al. (1995), which calibrates the uncertainty as a function of the measured TDR. This calibration was done independently for each observing run, and we find that our data are on the standard system to within 0.3 km s^{-1} . For the dynamical analysis presented in this paper, only stars with uncertainties of less than 5 km s^{-1} are used. Velocities were converted from the measured (heliocentric) values to the Galactic Standard of Rest after correcting for Earth barycentric motion, assuming a solar motion (in a right-handed, Cartesian coordinate system) of $(U, V, W)_{\odot} = (10.0, 5.2, 7.2) \text{ km s}^{-1}$ (Dehnen & Binney 1998), and using the IAU value of $\Theta_{LSR} = 220 \text{ km s}^{-1}$. The full data obtained

for each star are listed in Table 2, including the Sgr field name (col. 1), 2MASS ID and dereddened photometry (cols. 2-4), Schlegel et al.’s (1998) derived $E(B - V)$ for the star’s position (col. 5), Galactic coordinates (cols. 6 and 7), Sgr longitude, measured along the major axis (col. 8; Λ_{\odot} from PAPER I), the measured RV and uncertainty (cols. 9-10), the TDR (col. 11) and Sgr membership determination (col. 12; see §3.2).

Figure 2 shows the 2MASS CMDs of each field and the stars observed with reliably ($\langle\epsilon_V\rangle < 5$ km s $^{-1}$) measured RVs marked. Stars determined to be Sgr members (see below) are shown in blue, and those found to be non-members in black. As may be seen, RV members with a wide range of RGB magnitudes are sampled, but because we prioritized targets by magnitude, typically in the more densely populated fields these members are sampling temperatures primarily associated with M giant spectral types (i.e., $J - K \gtrsim 0.9$). For fields that sample lower density regions of the Sgr dwarf the RV members are drawn from the hotter, fainter part of the RGB where the luminosity function yields more potential candidates, including K spectral types.

3.2. Selecting Likely Sgr Members

We select stars likely to be associated with the Sgr core based solely on their RVs with respect to the Sgr mean. The field-by-field RV distribution of stars and the ultimate membership selections are shown in Figure 3. Likely Sgr member stars were selected in each field by using an iterative 3σ rejection technique including measurement uncertainties as fully described in Pryor & Meylan (1993). Due to the low numbers of Sgr members in the outer, lower Sgr density fields ($> +02$) a pre-selection ($90 < V_{GSR} < 220$ km s $^{-1}$) was made to eliminate obvious Galactic contamination, which is centered around $V_{GSR} \sim 25$ km s $^{-1}$. These membership evaluations for each star are included as the last column in Table 2.

The net census of RV-classified members and the derived kinematics for each field are compiled in Table 3, which shows the mean RV (col. 2), velocity dispersion (col. 3), radial distance of the field from the Sgr core (col. 4), elliptical distance of the field scaled to the major axis (col. 5), and the number of “member” stars used in the mean RV and dispersion determinations (col. 6). The derived mean, dispersion and total number of members is represented in Figure 3 as a (red) Gaussian with these properties. The actual distributions of Sgr members in each field are Gaussian at the 99% confidence level, except for two fields: Major+12, which has few stars, and NE+02.

3.3. Galactic Contamination

Sgr members selected to this point are those stars falling along the nominal Sgr RGB in 2MASS CMDs and having radial velocities within a reasonable range of expected values for the rather rapidly moving Sgr core. Nevertheless, it is possible that MW contaminants of identical color-magnitude combination might slip into our “member” list if they fall along the extreme tails

of the Galactic field star velocity distribution. While we cannot identify specific contaminants without further information, we can estimate the expected number of such stars using a model for the MW.

To this end, the distribution of velocities in each field was modeled using the Besançon MW model (Robin et al. 2003; see Table 4). For each field, the model output of the Galactic RV distribution for stars that satisfy our CMD selection (col. 2) was scaled to match the number of RV non-members in our spectroscopic sample for each field (col. 3) according to the ratio of the latter to the total CMD-qualifying Besançon stars (col. 4). From these scaled Besançon RV distributions (shown as blue lines in Fig. 3) we find the expected contamination as those stars falling in the adopted “RV member” range (col. 5). Compared to our “member” stars in each field (col. 6) we find the fractional contamination (col. 7) to be a minor effect except in three fields (Minor–03, Minor+05, and NW+04). This evaluation of a large contamination fraction in these fields conforms to a simple visual inspection of the scaled Besançon RV distributions in these fields (Fig. 3). We exclude these three fields from further analysis in this paper.

4. KINEMATICS OF THE SAGITTARIUS DWARF GALAXY CORE

4.1. Central and Global Velocity Trends

The velocity data derived in the previous section can be used to profile the trends of mean velocity and velocity dispersion across the Sgr core. First, we compare our *central* velocity dispersion to that obtained by Bellazzini et al. (2008), who provide high precision measurements of the inner 9' of Sgr and the globular cluster M54. We find that our center field velocity dispersion (Major+00; $9.85 \pm 0.73 \text{ km s}^{-1}$) is consistent with the dispersion they derive for Sgr *after* removing M54 ($9.60 \pm 0.40 \text{ km s}^{-1}$), which is expected given that our selection of stars is over a relatively large area. As a check on the effects that M54 would have, we also calculated the dispersion for the Major+00 field after removing the 33 stars in the area covered by Bellazzini et al. (2008; e.g., 9' radius around M54). The new dispersion ($9.90 \pm 0.81 \text{ km s}^{-1}$) shows that M54 has a negligible effect on our derived central velocity dispersion.

The only other large-area RV study of the Sgr core, though with lower velocity precision, is that of Ibata et al. (1997). Most of the Ibata et al. data were obtained using AAT/AUTOFIB, which resulted in per star uncertainties of $\sim 12 \text{ km s}^{-1}$ (i.e., of the same order as the Sgr core velocity dispersions). This lower precision probably results in the inflated near-center velocity dispersions obtained from these data (visible, e.g., in Figs. 4 and 6, gray open squares and open circles). Additional data were taken by Ibata et al. with CTIO/ARGUS at a higher precision, though the actual resulting uncertainties are not given by these authors (we estimate them to be $\sim 4 \text{ km s}^{-1}$ based on comparison to their repeat observations presented in their Table 2(b)). We find a smaller central velocity dispersion ($9.85 \pm 0.73 \text{ km s}^{-1}$) than Ibata et al. ($11.4 \pm 0.7 \text{ km s}^{-1}$), which, again, is likely explained by the high precision data of our study, and perhaps underestimated velocity

errors for the Ibata et al. ARGUS data. The Ibata et al. data are for stars around the center of Sgr with a couple outlying fields that fall near the major axis. For comparison, their dispersions are presented in our Table 3 and projected into the trends of our survey in Figures 4 and 6, which show a good correspondence.

Figure 4 shows the measured velocity and velocity dispersion trends versus both the straight projected radius as well as the elliptical radius (i.e., the radius normalized to the semi-major axis along the elliptical density contours using the shape determined in Majewski et al. 2003). We find a declining V_{GSR} trend as a function of radius in both R and R_e , however this format is not very sensible for interpreting the V_{GSR} trend, since it azimuthally averages over a general velocity trend along the satellite, one seen predominantly along the major axis (see below). The presence of a global V_{GSR} trend is evident by the distribution of mean velocities color-coded in the survey map shown in Figure 5 and discussed further below.

4.2. Testing for Rotation

In addition to looking at global radial trends, by exploiting our areal coverage we can explore trends along four different primary axes (major, minor, SW–NE, and NW–SE). This is particularly helpful for looking for a signature of Sgr rotation. Ibata et al. (1997) first looked for evidence that Sgr may show rotation along the minor axis as an effect of tidal stripping, after claims for rotation in Ursa Minor dSph were made (Hargeaves et al. 1994). Their data showed no evidence of minor axis rotation. More recently, Peñarrubia et al. (2010) predicted a Sgr core rotation as large as 20 km s^{-1} as a way to “naturally” produce a bifurcated leading arm among the Sgr tidal debris. Such a bifurcation is one explanation for the apparent double arms of Sgr debris in the northern Galactic hemisphere “field of streams” (Belakurov et al. 2006). Our data provide an excellent opportunity to re-verify the Ibata et al. claim for no measured rotation along an even greater span of the main body than they explored, and to test Peñarrubia et al.’s prediction of a rotating Sgr core.

To clarify the trends observed, it is beneficial to explore them as a function of position along the major and minor axes (Figure 6) as well as along the diagonal (Figure 7) axes across the center of Sgr. It is clear that our data show no significant gradient at all along the minor axis, in agreement with the data and suggestion by Ibata et al. (1997) for a lack of minor axis rotation. On the other hand, Figure 6 shows a clear global velocity gradient along the major axis, which could be a signature of rotation; however the observed trend is contrary to that proposed by Peñarrubia et al. Their models suggest that there should be an *increase* to $V_{GSR} \sim 180 \text{ km s}^{-1}$ along the major axis in the trailing arm direction, but we find a *decrease* to $V_{GSR} \sim 150 \text{ km s}^{-1}$. In addition, given the large area on the sky spanned by the major axis coverage other possibilities exist to explain these trends besides rotation; these are fully explored in §4.3 below. We see no significant trends in V_{GSR} along the other axes available to our survey (SW–NE and NW–SE), as explored further below.

Peñarrubia et al. (2011) have conducted their own radial velocity survey of Sgr specifically to

look for the Sgr rotation predicted by their earlier model and thereby test whether rotation can explain bifurcation seen in the Sgr tails. Similar to our findings here, these authors only find an RV trend along the major axis, and no evidence of minor axis rotation, though their coverage is more limited and only covers one side of the Sgr minor axis. Because the individual radial velocities from Peñarrubia et al. (2011) have not been published, a detailed analysis and comparison between our data sets is not yet possible.

4.3. Modeling Large Area Orbital Effects

To investigate in detail the kinematical trends seen within the Sgr core data, it is necessary to distinguish the effects of potential intrinsic rotation from global trends due to the motion of Sgr along its orbit, which, due to Sgr being observed over a large expanse of sky, leads to strong radial velocity variations as observed from Earth.

We therefore construct a two-dimensional velocity map by binning the velocity data into 1 deg² bins in the Sgr core coordinates, and compare this map to theoretical models. As shown in Figure 8 (upper left panel), the observational data show a statistically significant velocity gradient along the major axis of Sgr, with $v_{\text{GSR}} \approx 174 \text{ km s}^{-1}$ in the Major-04 field and $v_{\text{GSR}} \approx 152 \text{ km s}^{-1}$ in the Major+12 field. Such a trend can be expected even for a non-rotating model however, and reflects the changing projection of the space velocity of Sgr stars onto the line of sight with angular position across the dwarf. In Figure 8 (upper middle panel) we compare to the velocity trend expected if we were to adopt the simplest possible model for Sgr; namely an extended solid-body translating with space velocity $(U, V, W) = (230, -35, 195) \text{ km s}^{-1}$ (see Law & Majewski (2010b); LM10 hereafter), for which all variation of the radial velocity across the body is due to projection effects. The trend of radial velocities along the major axis in this simple solid-body model closely resembles the trend in the observational data, although the magnitude of the end-to-end velocity differential is significantly larger ($\sim 90 \text{ km s}^{-1}$) than observed (Figure 8, lower left panel).

A solid-body model is a poor descriptor of real, extended Galactic satellites however, because such satellites respond to the Galactic gravitational potential and unbound stars have streaming motions along the tidal streams. A more physically motivated comparison may be made to the N -body model of Sgr presented by LM10; this model assumes that Sgr was originally an isotropic (i.e., non-rotating) Plummer sphere and follows the orbits of the 10^5 individual tracer particles over the interaction history of the dwarf, thereby accounting for both projection effects and varying space velocities throughout the bound Sgr core and unbound tidal streams.¹ As illustrated in Figure 8 (upper right panel), the LM10 model also shows a significant velocity gradient along the major

¹While the LM10 model was not constrained to match the Sgr core in detail, its accuracy suffices for the present analysis. Due to numerical limitations of the N -body technique though, the LM10 model actually overshoots the current location of Sgr by $\sim 2^\circ$ along its orbit. We manually adjust the LM10 model back along its orbit to correct for this.

axis, but with an amplitude more similar to that of the observational data. Subtracting the LM10 model velocity field from the observational data, we construct a map of the radial velocity difference between the observational data and the non-rotating LM10 theoretical model (Figure 8, lower middle panel). In this velocity difference map, the remaining major-axis velocity gradient is no longer apparent, suggesting that the gradient in the observational data is due to orbital streaming motions rather than intrinsic rotation in the dwarf. Combining the observational uncertainties in the mean radial velocity for each field in quadrature with the corresponding uncertainty from the LM10 model fields, it is possible to convert the velocity difference map to a map of the statistical significance of deviations from the LM10 model (Figure 8, lower right panel). No obvious trends of positive/negative residuals are apparent, although we note that, intriguingly, the majority of observational fields with $r \gtrsim 3^\circ$ from the Sgr core have velocities lower than the LM10 model by $\sim 2 - 3\sigma$ (i.e., $\sim 5 - 10 \text{ km s}^{-1}$). The interpretation of this feature is uncertain, but the $r \sim 3^\circ$ boundary may indicate the transition from predominantly-bound to predominantly-unbound stars (expected to occur at $r \sim 4.5^\circ$ in the LM10 model), for which streaming motions might be slightly different than predicted.

In Figure 9, we evaluate the significance of the velocity residuals remaining along the major and minor axes after subtracting the LM10 model from the observational data. The residuals are best fit with a velocity gradient declining slightly along the major axis ($0.5 \text{ km s}^{-1} \text{ deg}^{-1}$) and minor axis ($1.2 \text{ km s}^{-1} \text{ deg}^{-1}$), but the reduced χ^2 of these fits are not significantly better than obtained with a constant velocity model.

As another way to look for an axis of rotation, we projected the mean velocities of all fields onto variously oriented axes through the Sgr center. We projected the stars onto axes rotated every degree starting with the major axis, and fit the velocities with a linear slope (0° and 180° are along the major axis and 90° is along the minor axis). We plot these fitted slopes as a function of axis angle in Figure 10. This analysis (Figure 10) shows no evidence of minor axis rotation (significant slope across the galaxy) with either model, again confirming the results of Ibata et al. (1997). After subtraction of either the solid body or the LM10 models, there is no significant rotation seen along *any* axis. At most possibly a slight trend mostly on the major axis is seen.

While it is not possible to completely rule out rotation at the level of a few km s^{-1} (given observational uncertainties and uncertainties inherent to the simple the solid-body model and fact that the LM10 does not try to explicitly fit the Sgr core), there is no compelling evidence for statistically significant rotation about either the major or minor axis (or any other axis) in the central $\sim 6^\circ$ of the Sgr dwarf. In particular, *we find no evidence* that Sgr has a strongly rotating ($\sim 20 \text{ km s}^{-1}$ amplitude) core, as predicted by Peñarrubia et al. (2010) for disk models of the Sgr progenitor that are capable of producing a bifurcation in the Sgr leading tidal stream. This point was previously made based on a simpler treatment of these same data by Lokas et al. (2010a) and using different data in Peñarrubia et al. (2011).

5. VELOCITY DISPERSION PROFILE IN THE PRESENCE OF DARK MATTER AND TIDAL DISRUPTION

5.1. Supplementary Data Bridging the Sgr Core and Tails

Because velocity dispersion profiles and how they bear on the mass profile of a dSph have become central to understanding the total mass and dark matter content of these systems, and because we wish to provide as similar a portrait of the dynamics of the Sgr core as we have for other dSphs, we have sought to append the dispersion profile of the Sgr system with data even farther from the Sgr core than provided in Figure 4. Thus, we have obtained additional spectra for a small sample of stars (shown in Figure 1) that bridge from the data shown in Figure 4 (which reach $0.47r_{lim}$, where r_{lim} is the limiting radius of a King profile fit to the density profile of the Sgr core, found by Majewski et al. 2003 to have the value $r_{lim} = 1801$ arcmin) to those velocity data previously published for unbound stars in the trailing arm by Majewski et al. (2004).

These supplementary data, which focused on the calcium infrared triplet spectral region, were obtained with the Modular Spectrograph and a 1200 line mm^{-1} grating on the DuPont 2.5-m telescope on the nights of UT 2003 Sep 19-20. The stars were selected as 2MASS M giants of the expected distance of Sgr (see Majewski et al. 2003) and lying near the semi-major axis of Sgr on its trailing side and cover the outer parts of the Sgr core, from 12.7° (i.e., $0.44r_{lim}$) to 48.2° (i.e., $1.6r_{lim}$). The positions of the selected stars are shown in Figure 1. Radial velocities were evaluated using the methodology discussed in Majewski et al. (2004; PAPER II), but — because these data were obtained with a slit spectrograph rather than with fibers — with the addition of a post-processing correction to each velocity that accounts for errors in the centering of each star on the slit (see discussion of this procedure in Sohn et al. 2007). These errors — typically amounting to a few km s^{-1} — were evaluated by measuring, via cross-correlation against a template of twilight sky, the relative position of telluric absorption features, including the A band and the series of H_2O and OH molecular lines near 8200 \AA , which directly map the stellar slit-centering error. Based on the measured RVs in multiply observed stars, we determine that these spectra, spanning $7700\text{--}8700 \text{ \AA}$ at a resolution of 1.7 \AA per resolution element, yield RV uncertainties after the telluric line corrections of effectively 2 km s^{-1} — i.e., well-suited to measuring σ_v 's and matching well the precision of the data we collected using Hydra (presented in Table 2).

The data for these supplementary stars are provided in Table 5. The full RV data for each star including 2MASS ID and dereddened photometry (cols. 1-3), Schlegel et al. (1998)-derived $E(B - V)$ (col. 4), Galactic coordinates (cols. 5 and 6), Sgr Λ_\odot coordinate (col. 7; see §2.1), RV and uncertainty (cols. 8-10), height of the cross-correlation peak (col. 11), data quality (col. 12; see Paper II for definition of this quantity, which goes from 0 [worst] to 7 [best]), and membership (col. 13; have RVs consistent with being members of the most recently detached part of the trailing arm). A simple scan down the V_{GSR} column of Table 5 shows that only about 5 of the 37 stars observed with the DuPont have RVs inconsistent with being members of the most recently detached part of the trailing arm (though it is possible that a few of the stars could be Sgr stars from other wraps

of tidal debris, particularly at the largest separation from the Sgr center — see, e.g., PAPER II). Grouping the remaining 32 stars into 3 additional radial bins (e.g., Figure 11) enables us to follow the RV dispersion profile of Sgr to the King limiting radius (30°) of the King profile fit to Sgr in PAPER I.

5.2. Velocity Dispersion Trends

The distribution of the velocity *dispersion* as a function of radius (either strictly circular or elliptical) shown in Figure 4 is the typical way that dSph dynamics and mass profiles are explored. As may be seen, the velocity dispersion of Sgr remains more or less flat to the limit of our study, albeit with a colder dispersion in the very center. This cold point is not seen in the poorer resolution AAT data of Ibata et al. (2007), but is seen in their better precision ARGUS data and confirmed also by the high resolution Bellazzini et al. (2008) data (see §4.1). The upper panel of Figure 6, which shows the data only for fields along the major axis of Sgr, demonstrates the cold point most clearly.

A single field, Minor+03, shows an anomalously high velocity dispersion, by almost a factor of two compared to other fields nearby or symmetrically placed around the Sgr main body. Though the contamination of this measurement by MW stars is not estimated to be abnormally high (Table 4), inspection of Figure 3 suggests that the actual situation may be worse than this, in that, like the fields already thrown out of our analysis (Minor−03, Minor+05, and NW+04), the “Sgr RV peak” in Minor+03 is the most overlapped by the distribution of MW field stars in the same field. It would not be surprising to be concerned about Minor+03 if Minor−03 is untrustworthy, given the likely similar Sgr density in these symmetrically placed fields, but an even higher expected MW presence in Minor+03, which is located even closer to the Galactic mid-plane. Thus, we put no confidence in the measured velocity dispersion in the Minor+03, and exclude it from further analyses.

We conclude that there is no evidence for “sub-structure” or features in the dispersion profile — other than the central cold point. The velocity dispersion remains more or less constant as far as it can be probed, even when we include the DuPont data at farther radii (§5.1), as shown in Figure 11. Obviously Figure 11 maps the Sgr dynamics from the bound inner regions of Sgr out into the regions dominated by unbound tidal debris, wherever that occurs. And yet no obvious evidence for any change in the profile due to that transition can be discerned.

Similar velocity dispersion profiles to that mapped here for Sgr have been seen in the modeling of the cores of dark matter-dominated dSph galaxies experiencing tidal disruption by Muñoz et al. (2008). Those models were specifically designed to match the properties of the Carina dSph, which in density distribution and velocity dispersion profile greatly mimics what is observed in Sgr. As shown in those models, the flat velocity dispersion is a reflection of the presence of unbound stars, and, as shown there, the transition from a system dominated by bound particles to one dominated by unbound particles generally shows no feature in the velocity dispersion profile when all stars in

the simulations are used, and a sigma-clipping rejection, similar to the one used for real data, is applied.²

This trend of flat line-of-sight velocity dispersion profiles to the limit of where kinematical data exist is also observed for all other “classical” MW dSphs (Muñoz et al. 2005, 2006; Walker et al. 2006, 2007; Koch et al. 2007; Mateo et al. 2008; see Figure 12). Given the predominance of unbound debris well inside the King limiting radius in the case of Sgr (e.g., see §4.3.3 of Majewski et al. 2003), the overall similarity of its velocity dispersion profile to those of other dSphs over similar radii is either an important structural clue or an unfortunate, confounding coincidence. The flatness of the dispersion profiles in other dSphs has been interpreted as evidence that mass in these systems does not follow the light (e.g., Kleyana et al. 2002, Lokas et al. 2005, Mashchenko et al. 2005, Gilmore et al. 2007; Koch et al. 2007; Walker et al. 2007) and moreover, that they are surrounded by larger dark matter halos. However, that a system like Sgr, so clearly undergoing tidal stripping, shows an identical behavior in its velocity dispersion profile, even including that portion of the system almost surely dominated by its unbound stellar component, provides us, at minimum, with a cautionary example regarding the derivation and interpretation of dSph mass profiles and assumptions about the extent of the bound component.

6. DISCUSSION

6.1. Summary of Sgr Core Properties Found Here

We have conducted the first large scale systematic survey of the Sgr dSph main body with broad azimuthal coverage. Using over 1200 member stars, we are able to investigate evidence for effects that would be seen over large areas, such as rotation and global velocity dispersion trends. A complementary study of the metallicity distribution across Sgr using these same spectra will be included in a future contribution.

The primary results from this paper may be summarized as follows:

1. The Sgr central velocity dispersion is found to be $9.9 \pm 0.7 \text{ km s}^{-1}$, in agreement with the dispersion ($9.6 \pm 0.4 \text{ km s}^{-1}$) found by Bellazzini et al. (2008) after removing stars associated with M54 (e.g., Figure 4, §4). This central velocity dispersion is not atypical among the “classical” dSph galaxies (see Table 6).

2. Within the distribution of radial velocities, we find no signatures of rotation along the minor axis of Sgr. With a detailed investigation of trends along the major axis, we find evidence for at most a small trend ($\leq 4 \text{ km s}^{-1} \text{ deg}^{-1}$), though even this small effect can be explained without

²If one studies the behavior of the bound and unbound components separately, then the difference in behavior is evident, with the bound part decreasing with radius and the unbound part remaining flat or rising depending on the specific model, a phenomenon also shown by Klimentowski et al. (2007).

needing intrinsic rotation, as shown by various adopted models of an extended Sgr system moving along its orbit. Thus, we confirm that Sgr is like other dSphs in having no significant rotation ($v_{rot}/\sigma(v) \gtrsim 1$) signature along any axis (e.g., Figures 10, §4).

6.2. Consistency with the Tidal Stirring Model

In a companion study by Lokas et al. (2010a), N -body simulations were generated to explain both the elongated shape and velocity characteristics (as found in the present study) of the Sgr core. Of critical significance to the model described there was that the present study found no significant rotation curve across the face of the dSph, which supports the notion that Sgr is bar-like with the major axis almost perpendicular to the line of sight, not a disk seen almost edge-on, which would exhibit a significant rotational signal. The bulk of the small observed rotation is simply due to projection effects, and the insignificant intrinsic rotation of the system points toward a prolate shape for the galaxy, a configuration supported by radially-orbiting stars. A disk-like configuration was recently employed by Peñarrubia et al. (2010) as an intriguing way to produce a bifurcated leading arm (as a means to explain the two Sgr streams seen in the Sloan Digital Sky Survey data — Belokurov et al. 2006; Yanny et al. 2009), but the 20 km s^{-1} level of rotation expected to be seen today in such a model is clearly precluded by the present observations, a point also made by Peñarrubia et al. (2011) from observations they made to test their model (over a smaller area than covered here).

On the other hand, as shown in Lokas et al. (2010a), the data presented here are consistent with the model of tidal stirring (Mayer et al. 2001; Klimentowski et al. 2007, 2009; Kazantzidis et al. 2011) proposed there to account for the shape and dynamics of the Sgr core. According to the proposed scenario, dwarf galaxies like Sgr did indeed start out as disk-like systems (embedded in extended dark matter halos), but in the presence of the tidal field of a larger host galaxy like the MW, these systems are transformed into spheroids via formation and subsequent shortening of a bar, and through this process the stellar motions are altered from ordered to random. Depending on what phase of this dynamical transformation the dwarf galaxy is viewed, it can be highly elongated (e.g., just after bar formation) to very spherical (e.g., much further evolved). The best fitting model for the Sgr case explored by Lokas et al. places the presently observed phase just beyond the second perigalacticon, intermediate between the phase of bar formation at first perigalacticon (a phase where Sgr would have tidal arms too short) and the third perigalacticon (a phase where Sgr would be spherical).

This is the first model to explain both the very large ellipticity of Sgr as well as the observed kinematics of its stars, but presupposes that the current Sgr orbit is a recent product of dynamical friction from a larger orbit having an apocenter exceeding 100 kpc on which Sgr was deposited after cosmological infall into the MW halo. This orbital evolution could occur if the initial mass of the system was large — similar to that of the Large Magellanic Cloud, a system itself that has probably only recently been accreted (e.g., Besla et al. 2007) and that presently contains a bar, a

morphology consistent with the early phases of the proposed evolutionary scenario. Coincident with the orbital erosion from dynamical friction, the Sgr system must have shed a significant amount of mass, mostly dark matter, but also probably baryons, to bring it to its presently smaller size; a large, LMC-mass progenitor would be required to achieve a significant amount of orbital erosion (Colpi et al. 1999; Jiang & Binney 2000; Taffoni et al. 2003). That the LMC may be an apt model for the Sgr progenitor is supported by the similarity in extended star formation histories (e.g., Siegel et al. 2007; Harris & Zaritsky 2009) and detailed chemical evolution (Chou et al. 2010). Indeed, as we reiterate from Lokas et al. (2010a), the primary difference in the present appearance of the LMC and Sgr may well have to do with timing — i.e., the phase of dynamical evolution dictated by the relative orbital sizes and times they have been bound to the MW.³

6.3. Is the Disrupting Sagittarius Galaxy a Dwarf Spheroidal Exception or Rosetta Stone?

In the previous section we made a connection of the Sgr system to dwarf irregular/dwarf spiral galaxies via dynamical evolution models with tidal stirring and through observed similarities in star formation and enrichment history. But how does Sgr fit within the context of the dwarf spheroidal galaxies with which it is normally morphologically classified, and what does it potentially tell us about the origin and evolution of these systems?

More than seventy years after their discovery, there still remains no universally agreed upon, complete picture of the nature of dwarf spheroidal (dSph) galaxies. Hodge (1964a, 1961b, 1962, 1966) and Hodge & Michie (1969) first invoked tidal effects to explain the diffuse structure of at least some dSphs. On the other hand, ever since the work of Aaronson (1983) to derive the first radial velocity dispersion (σ_v) of a dSph, the notion that they are laden with dark matter (DM) has emerged as the standard paradigm to explain the observed structure and dynamics of these systems.

In the last decade, enormous efforts have been plied to collecting data on dSphs to their greatest radial extent. Evidence for very distended structure has been reported for the classical (i.e., the most luminous, not including the “ultrafaints”) MW dSphs (e.g., Majewski et al. 2000; Martinez-Delgado et al. 2001; Palma et al. 2003; Westfall et al. 2006; Muñoz et al. 2006; Sohn et al. 2006; some of these data are collected in Figure 13). These observed morphologies might be

³For example, Sgr differs from the LMC in being presently devoid of gas, but the former clearly had gas as recently as ~ 0.75 Gyr ago to create its youngest stellar population (Siegel et al. 2007). That last star formation episode may well have depleted Sgr’s gas reservoir, and/or other processes — such as ram pressure stripping or supernovae blowout — may have contributed. All three processes — (1) gas depletion, (2) ram pressure stripping, and (3) supernovae blowout — are conceivably accelerated in the case of Sgr because of (1) more frequent and intense tidal shocking to produce starbursts at its smaller orbital radius, (2) the higher density of the ram pressure medium at this orbital radius, or (3) the weakened binding energy for the more dynamically evolved, tidally diminished Sgr core.

used to infer either that dSphs are being tidally disrupted, with the stripped stars accounting for the extended structures (the general view of the above cited sources; see also Lokas et al. 2008), or that the dSphs are *very* large, fully internally-bound, massive structures (e.g., Gilmore et al. 2007; Wu 2007).⁴

The latter view has often been bolstered by the advent of spectroscopic studies that have collected hundreds, and in some cases thousands, of individual radial velocities over much of the luminous extent of dSphs. These new data sets have revealed flat or just slowly rising/declining velocity dispersion profiles all the way to the limits of where data exist (e.g., Westfall et al. 2006; Sohn et al. 2006; Muñoz et al. 2006; Walker et al. 2007 — some of these data are summarized in Fig. 12), a behavior that might be reasonably well explained by the assumption that dSphs live inside much larger DM halos in dynamical equilibrium (e.g., Kleyana et al. 2002; Lokas 2002; Lokas et al. 2005; Maschenko et al. 2005; Gilmore et al. 2007; Koch et al. 2007; Wu 2007; Walker et al. 2007) and resulting in dramatically rising mass-to-light ratios with radius and large inferred total satellite masses.

However, as argued by Muñoz et al. (2005, 2006), the extent of some of the mapped dSphs, as verified through RV-membership studies of extreme outlying stars in the luminosity profiles, imply very large linear dimensions, mass-to-light ratios, and total masses if all of the identified outer stellar members are assumed to be bound; for example, in the case of Carina, Muñoz et al. obtain $M/L > 16,000$, $M_{dSph} = 7.2 \times 10^9$ and $R_{tidal} \sim 4$ kpc to keep the outermost RV-member star bound. While there is currently debate about whether M/L ratios this large make sense for the classical MW dSphs — e.g., whether they sit in the largest DM subhalos seen in simulations or in systematically smaller halos (Ferrero et al. 2011; Boylan-Kolchin et al. 2011) — the above-implied dimensions for Carina rival those of the Magellanic Clouds and are not likely to hold universally for all classical MW dSphs based on expected subhalo mass spectra (e.g., Moore et al. 1999). It seems even less likely that these dimensions would hold, just by chance, for the first few examples of dSphs that have received the most radially extensive observational attention.

Alternatively, the observed flat velocity dispersion profiles up to and beyond the observed King limiting radii, r_{lim} , of these systems might also be taken as further proof for a more universal tendency for the classical MW dSphs, while containing DM to be sure, to be experiencing tidal disruption of their luminous parts as well. It is now well established that the MW halo contains extensive stellar substructure from hierarchically merged “subhalos”, and dSph galaxies are prime candidates for the progenitors of these substructures. Moreover, Sohn et al. (2006); Muñoz et al. (2008); Lokas et al. (2008, 2010b), among others, have successfully produced N -body simulations

⁴In a study of the Sculptor dSph, Coleman et al. (2005a) suggest yet another interpretation of the extended structure as one relating to variations in the distribution of stellar populations; nevertheless these authors do not rule out the possibility that a small extratidal component may exist in this system. Meanwhile, Coleman et al. (2005b) identify an apparent excess of stars around the Fornax system as due to the remains of another, smaller satellite that previously merged with Fornax.

of DM-filled, tidally disrupting, mass-follows-light satellites that well match the observed properties of the Carina and Leo I dSphs — two of the three dSph systems (apart from Sgr) with the most extensive radial coverage in their velocity mappings. Similar models are also seen to work for Fornax, Sculptor and Sextans (Lokas 2009).

Here we lend further support to this morphological and evolutionary paradigm from a decidedly phenomenological point of view. Figure 13, a synthesis of previous structural studies (see references above), clearly demonstrates the similarity of the Sgr *morphology* to that of other dSphs — i.e., an inner King profile with, at the largest radii, an extended, slower declining “break⁵ population” — whereas the present study demonstrates quite vividly that the Sgr dwarf galaxy, *a DM-dominated system that nonetheless is demonstrably undergoing tidal disruption*, also has observed kinematics strongly resembling those of the other classical MW dSph galaxies. Of course, the lack of any significant rotation in Sgr is commensurate with the kinematics of other dSphs. But, in addition, as Figure 12 demonstrates (data from Muñoz et al 2005, 2006; Walker et al. 2007; and Sohn et al. 2006), the velocity dispersion profile for Sgr as a function of radius for the data presented in this study also strongly imitates those for other MW dSphs. Just like the velocity dispersion profiles of the other classical MW dSphs, that of Sgr remains more or less flat to large radii, including that part of the system where it is clearly dominated by tidal debris.

As may be seen from the compilation of properties of the classical MW dSph systems in Table 6, Sgr is at one extreme within this group in terms of its distance, luminosity, linear size, ellipticity and derived mass, which might merit it being considered “exceptional” among the group. However, while Sgr is the most luminous and most massive dSph, it is not significantly brighter or more massive than Fornax, and its central velocity dispersion is similar to those of Sculptor, Draco, Ursa Minor, and Leo I and less than that of Fornax. Sgr also has an extended star formation history, like Fornax, Carina, Sculptor, Sextans, Leo I and Leo II. Meanwhile, we would argue that Sgr’s large ellipticity and half-light radius may well be a function of its presently small Galactocentric distance: As discussed above (§6.2) the ellipticity may be due to the recent infall of the system to a small orbit that induced tidal stirring, whereas the large present size may be due to Sgr recently experiencing catastrophic tidal disruption and mass loss, as argued by Chou et al. (2007).

Indeed, guided by the remarkable morphological and dynamical similarity of Sgr to the other MW dSph systems as well as its compatibility with the tidal stirring model, we conclude that Sgr may sometimes appear to be a “dSph outlier” simply because it is presently in a more flashy, but intermediate phase of a more universal evolutionary sequence from a disk, star-forming, “LMC-like” state to a more spherical, staid, dwarf spheroidal state long past active star formation, like the Draco system. As shown by Lokas et al. (2010a, 2011), the exact timescale for a dSph to follow this evolution is a function of its mass and orbital size, with the latter, of course, a function of the former through dynamical friction and the zero-age of the evolution set by the epoch of initial infall into the MW. In the case of Sgr, its present relative “flashiness” is driven by its currently small orbit

⁵That is, “breaking away” from the King profile.

(which amplifies the tidal stirring effect), proximity to perigalacticon (the most dramatic phase of both tidal stirring and mass loss), and its having recently formed significant stellar tidal tails (again, a function of the stronger tidal force experienced on the smaller orbit). If star formation history and morphology present ersatz timestamps of this “universal” evolutionary sequence (admittedly crude timestamps, because of the vagaries of viewing perspective, orbital shape, stochasticity of star formation histories, and initial conditions), then perhaps the less bar-like (Lokas et al. 2012) and recently star forming Fornax system may be another system in a somewhat earlier phase of transformation, while Carina and Leo I may be in a somewhat later phase. This proposed paradigm of a universal evolutionary track for tidally-stirred, infalling galaxies is explored in more detail, as a function of more parameters and including all Local Group galaxies in Lokas et al. (2011).

Our primary point here is that because Sgr offers a clear example *already found in nature* of a disrupting dwarf galaxy system containing DM that shares so many properties — e.g., density profile, lack of rotation, σ_v profile — with other classical, DM-filled MW dSphs that it is worth considering that the paradigms of not only tidal influence (e.g., stirring), but tidal *disruption*, may apply more ubiquitously to these other (classical) dSphs and that perhaps these other objects are also suffering varying degrees of tidal disruption, along the Sgr paradigm. In fact, as found by Lokas et al. (2010a), morphological transformation and mass loss take place together. Thus, we contend that tidal disruption, as in the case of Sgr, remains a viable explanation for the observed kinematics and structure at large radii of these other dSphs (as already suggested by e.g., Kuhn et al. 1996; Majewski et al. 2000; Palma et al. 2003; Westfall et al. 2006; Muñoz et al. 2006; Sohn et al. 2007; Mateo et al. 2008; Lokas et al. 2008 and modeled as DM-dominated but tidally influenced systems by, e.g., Sohn et al. 2007; Muñoz et al. 2006, 2008; Lokas et al. 2008). Indeed, with Sgr a widely-accepted representative of the tidal debris model, but with good cases in hand also for the Carina and Leo I systems (modeled well by even simple mass-follows-light DM models), one may well question the need to have a second explanation — i.e., large, extended DM halos to keep the observed extended stellar distributions bound and dynamically hot — to explain the outer structure of the other classical MW dSphs. In the least, if there are two mechanisms responsible for the outer structure and dynamics of dSphs, our results here show that dynamical studies are hard pressed to discriminate them.

Moreover, our analysis of the kinematics of the Sgr system demonstrate clearly that flat velocity dispersion profiles do *not* prove the existence of extended DM halos around dSphs. On the other hand, tidal tails, seen morphologically and not just inferred from kinematics, prove when extended DM halos are not present. Thus, one clear means by which we might hope to distinguish between structural/dynamical models — i.e., extended DM halos versus unbound tidal debris — for specific dSphs is to build more extensive and refined morphological maps capable of detecting (subtle) tidal tails. A more sensitive and systematic search for evidence of tidal tails around the Galactic dSph population would help build tighter empirical constraints on their true masses and help answer the questions of whether dSphs typically live in truly huge ($10^{10-11} M_\odot$) DM subhalos or smaller ones and what this implies for the efficiency of galaxy formation on these scales (Ferrero et al. 2011;

Boylan-Kolchin et al. 2011).

In conclusion, in contrast to the way Sgr is often portrayed in studies of MW dSphs (see Section 1), we argue that it may not be an anomaly, but rather a Rosetta Stone of dSph galaxies and their evolution in a MW-like environment. Perhaps Sgr’s only overriding exceptional quality is that it is the MW dSph presently in the most dramatic stages of a universal evolutionary path that includes tidal harassment and tidal disruption.

We acknowledge funding by NSF grant AST-0307851, NASA/JPL contract 1228235, the David and Lucile Packard Foundation, and the F.H. Levinson Fund of the Peninsula Community Foundation. PMF was supported by an NSF Astronomy and Astrophysics Postdoctoral Fellowship under award AST-0602221, the NASA Graduate Student Researchers Program, a University of Virginia Faculty Senate Dissertation-Year Fellowship. RRM acknowledges support by the GEMINI-CONICYT Fund, allocated to the project No. 32080010 and from CONICYT through projects FONDAP N15010003 and BASAL PFB-06. ELL is supported by the Polish National Science Centre grant no. N N203 580940.

REFERENCES

- Aaronson, M. 1983, *ApJ*, 266, L11
- Amandroff, T.E. & Zinn, R. 1988, *AJ*, 96, 92
- Bellazzini, M., Gennari, N., Ferraro, F. R., Sollima, A. 2004, *MNRAS*, 354, 708
- Bellazzini, M., Ferraro, F. R., Origlia, L., Pancino, E., Monaco, L., Oliva, E. 2004, *AJ*, 124, 3222
- Bellazzini, M., et al. 2008, *AJ*, 136, 1147
- Belokurov, V., et al. 2006, *ApJ*, 642, 137
- Besla, G., Kallivayalil, N., Hernquist, L., Robertson, B., Cox, T.J., van der Marel, R.P., Alcock, C. 2007, *ApJ*, 668, 949
- Bessell, M. S., & Brett, J. M. 1988, *PASP*, 100, 1134
- Binney, J. & Merrifield, M. 1998 *Galactic Astronomy*, Princeton Univ. Press, p.628
- Bonifacio, P., Hill, V., Molaro, P., Pasquini, L., Di Marcantonio, P., & Santin, P. 2000, *A&A*, 359, 663
- Bonifacio, P., Sbordone, L., Marconi, G., Pasquini, L., & Hill, V. 2004,, *A&A*, 414, 503
- Boylan-Kolchin, M., Bullock, J. S., & Kaplinghat, M. 2011, arXiv:1111.2048

- Carretta, E., et al. 2010, *A&A*, 520, 95
- Cenarro, A.J., Cardiel, N., Gorgas, J., Peletier, R.F., Vazdekis, A. & Prada, F. 2001, *MNRAS*, 326, 959
- Cenarro, A.J., Gorgas, J., Cardiel, N., Pedraz, S., Peletier, R.F. & Vazdekis, A. 2001, *MNRAS*, 326, 981
- Chou, M.-Y., et al. 2007, *ApJ*, 670, 346
- Chou, M.-Y., Cunha, K., Majewski, S.R., Smith, V.V., Patterson, R.J., Martínez-Delgado, D., & Geisler, D. 2010, *ApJ*, 708, 1290
- Cole, A. A., Smecker-Hane, T. A., Tolstoy, E., Bosler, T. L. & Gallagher, J. S. 2004, *MNRAS*, 347, 367 (CSTBG)
- Colpi, M., Mayer, L., Governato, F. 1999, *ApJ*, 525, 720
- Denhen, W. & Binney, J.J. 1998, *MNRAS*, 298, 387
- Ferrero, I., Abadi, M. G., Navarro, J. F., Sales, L. V., & Gurovich, S. 2011, arXiv:1111.6609
- Frinchaboy, P.M., Muñoz, R.R., Phelps, R.L., Majewski, S.R. & Kunkel, W.E. 2006, *AJ*, 131, 922
- Frinchaboy, P.M. & Majewski, S.R. 2008, *AJ*, 136, 118
- Gallart, C., Monelli, M., Dolphin, A., Bernard, E., Drozdovsky, I., Aparicio, A., & Cassisi, S. 2007, “From Stars to Galaxies: Building the Pieces to Build Up the Universe”, *ASP Conference Series*, 374, eds. A. Vallenari, R. Tantaló, L. Portinari, & A. Moretti, 253
- Gilmore, G. 2007, *From Stars to Galaxies: Building the Pieces to Build Up the Universe*, 374, 209
- Gilmore, G., Wilkinson, M. I., Wyse, R. F. G., et al. 2007, *ApJ*, 663, 948
- Grebel, E.K. 2004, in *Origin and Evolution of the Elements*, p. 234.
- Hargreaves, J. C., Gilmore, G., Irwin, M. J., & Carter, D. 1994, *MNRAS*, 271, 693
- Harris, J., & Zaritsky, D. 2009, *AJ*, 138, 1243
- Hodge, P. W. 1961a, *AJ*, 66, 249
- Hodge, P. W. 1961b, *AJ*, 66, 384
- Hodge, P. W. 1962, *AJ*, 67, 125
- Hodge, P. W. 1966, *AJ*, 71, 204
- Hodge, P. W., & Michie, R. W. 1969, *AJ*, 74, 587

- Ibata, R. A., Gilmore, G., & Irwin, M. J. 1994, *Nature*, 370, 194
- Ibata, R. A., Gilmore, G., & Irwin, M. J. 1995, *MNRAS*, 277, 781
- Ibata, R. A., Wyse, R. F. G., Gilmore, G., Irwin, M. J., & Suntzeff, N. B. 1997, *AJ*, 113, 634
- Irwin, M., & Hatzidimitriou, D. 1995, *MNRAS*, 277, 1354 (IH95)
- Jiang, I.-G., & Binney, J. 2000, *MNRAS*, 314, 468
- Kazantzidis, S., Lokas, E. L., Callegari, S., Mayer, L., & Moustakas, L. A. 2011, *ApJ*, 726, 98
- Kleyna, J., Geller, M., Kenyon, S., & Kurtz, M. 1999, *AJ*, 117, 1275
- Kleyna, J. T., Wilkinson, M. I., Evans, N. W., Gilmore, G., & Frayn, C. 2002, *MNRAS*, 330, 792
- Klimentowski, J., Lokas, E. L., Kazantzidis, S., Prada, F., Mayer, L., & Mamon, G. A. 2007, *MNRAS*, 378, 353
- Klimentowski, J., Lokas, E. L., Kazantzidis, S., Mayer, L., & Mamon, G. A. 2009, *MNRAS*, 397, 2015
- Koch, A., Kleyna, J.T., Wilkinson, M.I., Grebel, E.K., Gilmore, G.F., Evans, N.W., Wyse, R.F.G., & Harbeck, D.R. 2007, *AJ*, 134, 566
- Kroupa, P. 1997, *New Astronomy*, 2, 139
- Kuhn, J. R., Smith, H. A. & Hawley, S. L. 1996, *ApJ*, 469, L93
- Law, D.R. & Majewski, S.R. 2010, *ApJ*, 714, 229
- Law, D.R. & Majewski, S.R. 2010, *ApJ*, 714, 229
- Layden, A. C., & Sarajedini, A. 2000, *AJ*, 119, 1760
- Lee M.G., et al. 2003, *AJ*, 126, 2840
- Lokas, E. L., 2002, *MNRAS*, 333, 697
- Lokas, E. L. 2009, *MNRAS*, 394, L102
- Lokas, E. L., Klimentowski, J., Kazantzidis, S., & Mayer, L. 2008, *MNRAS*, 390, 625
- Lokas, E. L., Kazantzidis, S., Majewski, S. R., Law, D. R., Mayer, L., & Frinchaboy, P. M. 2010a, *ApJ*, 725, 1516
- Lokas, E. L., Kazantzidis, S., Klimentowski, J., Mayer, L., & Callegari, S. 2010b, *ApJ*, 708, 1032
- Lokas, E. L., Kazantzidis, S., & Mayer, L. 2011, *ApJ*, 739, 46

- Lokas, E. L., Majewski, S. R., Kazantzidis, S., Mayer, L., Carlin, J. L., Nidever, D. L., Moustakas, L. A. 2012, *ApJ*, 751, 61
- Lokas, E.L., Mamon, G.A., and Prada, F. 2005, *MNRAS*, 363, 918
- Majewski, S.R., Ostheimer, J.C., Kunkel, W.E. & Patterson, R.J. 2000, *AJ*, 120, 2550
- Majewski, S.R., Skrutskie, M.F., Weinberg, M.D. & Ostheimer, J.C. 2003, *ApJ*, 599, 1082
- Majewski, S. R., et al. 2004, *AJ*, 128, 245
- Martínez-Delgado, D., Alonso-García, J., Aparicio, A., & Gómez-Flechoso, M. A. 2001, *ApJ*, 549, L63
- Mashchenko, S., Couchman, H. M. P., and Sills, A. 2005, *ApJ*, 624, 726
- Mateo, M., Olszewski, E. W., & Walker, M. G. 2008, *ApJ*, 675, 201
- Mayer, L., Governato, F., Colpi, M., et al. 2001, *ApJ*, 559, 754
- McConnachie, A.W., Peñarrubia, J., & Navarro, J.F. 2007, *MNRAS*, 380, L75
- Mighell, K.J. & Burke, C.J. 1999, *AJ*, 118, 366
- Monaco, L., et al. 2005, *A&A*, 441, 141
- Monaco, L., Bellazzini, M., Bonifacio, P., Buzzoni, A., Ferraro, F. R., Marconi, G., Sbordone, L., & Zaggia, S. 2007, *A&A*, 464, 201
- Moore, B., Ghigna, S., Governato, F., et al. 1999, *ApJ*, 524, L19
- Muñoz R. R., et al. 2005, *ApJ*, 631, L137
- Muñoz R. R., et al. 2006, *ApJ*, 649, 201
- Muñoz, R.R., Majewski, S.R., & Johnston, K.V. 2008, *ApJ*, 679, 346
- oden01] Odenkirchen, M., et al. 2001, *AJ*, 122, 2538
- Palma, C., Majewski, S. R., Siegel, M. H., Patterson, R. J., Ostheimer, J. C., & Link, R. 2003, *AJ*, 125, 1352
- Peñarrubia, J., et al. 2010, *MNRAS*, 408, L26
- Peñarrubia, J., et al. 2011, *ApJ*, 727, L2
- Pietrzyński, G., et al. 2008, *AJ*, 135, 1993
- Pryor, T. & Meylan, G., 1993, in “Structure and Dynamics of Globular Clusters”, eds. by Meylan and Djorgovski, ASP Conference Series, 50, 357.

- Rizzi, L., Held, E.V., Saviane, I., Tully, R.B., Gullieuszik, M. 2007, MNRAS, 380, 1255
- Robin, A.C., Reylé, C., Derrière, S., & Picaud, S. 2003, A&A, 409, 523
- Sbordone, L., Bonifacio, P., Buonanno, R., Marconi, G., Monaco, L., & Zaggia, S. 2007, A&A, 465, 815
- Schlegel, D.J., Finkbeiner, D.P., & Davis, M. 1998, ApJ, 500, 525
- Siegel, M. H. & Majewski, S. R. 2006, Astronomical Society of the Pacific Conference Series, 352, 285
- Siegel, M. H., Majewski, S. R., Sohn, S. T., Shetrone, M. D., & Patterson, R. 2007, ApJ, 667, L57
- Siegel, M. H., Majewski, S. R., Law, D. R., et al. 2011, ApJ, 743, 20
- Skillman, E.D., Côté S., & Miller, B.W. 2003, AJ, 125, 593
- Smecker-Hane, T. A., & McWilliam, A. 2002, preprint (astro-ph/0205411)
- Smecker-Hane, T.A., Marsteller, B., Cole, A., Bullock, J., & Gallagher, J.S. 2009, BAAS, 41, 235
- Skrutskie, M.F., et al. 2006, AJ, 131, 1163
- Sohn, S., et al. 2007, ApJ, 663, 960
- Taffoni, G., Mayer, L., Colpi, M., & Governato, F. 2003, MNRAS, 341, 434
- Tolstoy, E., et al. 2004, ApJ, 617, L119
- Tonry, J. & Davis, M. 1979, AJ, 84, 1511
- Vogt, S.S., Mateo, M., Olszewski, E.W. & Keane, M.J. 1995, AJ, 109, 151
- Walker, M. G., Mateo, M., Olszewski, E. W., et al. 2006, AJ, 131, 2114
- Walker, M.G., Mateo, M., Olszewski, E.W., Gnedin, O.Y., Wang, X., Sen, B., Woodroffe, M. 2007, ApJ, 667, L53
- Walker, M. G., Mateo, M., Olszewski, E. W., Sen, B., & Woodroffe, M. 2009, AJ, 137, 3109
- Walker, M. G., Mateo, M., Olszewski, E. W., Olszewski, E.W., Peñarrubia, J., Wyn Evans, N., Gilmore, G. 2010, ApJ, 710, 886
- Weisz, D. R., et al. 2011, ApJ, 739, 5
- Westfall, K.B., Ostheimer, J. C., Majewski, S. R., Patterson, R. J., Frinchaboy, P. M., Link, R. & Kunkel, W. E. 2006, AJ, 131, 357
- Wu, X., 2007, ApJ submitted, arXiv:astro-ph/0702233v1

Yanny, B., Newberg, H. J., Johnson, J. A., et al. 2009, ApJ, 700, 1282

Zaggia, S., et al. 2004, Mem. Soc. Astron. Italiana Suppl., 5, 291

Table 1. Field Pointings in Galactic and Sgr Core Coordinates

Field	Λ_{\odot}^a	B_{\odot}^a	l	b	$\alpha_{(2000)}$	$\delta_{(2000)}$	$\langle E(B - V) \rangle_{Phot}^b$	$\langle E(B - V) \rangle_{Spec}^c$
Major+00	0.115	1.615	5.51	-14.21	18:55:24.29	-30:36:54.0	0.151	0.154
Major-04	355.992	1.221	4.92	-10.11	18:37:03.48	-29:26:30.7	0.201	0.197
Major-02	358.148	1.454	5.20	-12.26	18:46:34.41	-30:06:03.5	0.200	0.170
Major+02	1.937	1.655	5.91	-15.99	19:03:44.36	-30:57:06.0	0.175	0.121
Major+04	3.873	1.777	6.26	-17.90	19:12:36.40	-31:21:11.1	0.100	0.101
Major+06	5.982	2.082	6.47	-20.02	19:22:15.04	-31:55:09.0	0.122	0.119
Major+08	7.969	2.464	6.57	-22.04	19:31:23.80	-32:30:29.5	0.089	0.088
Major+10	9.992	2.658	6.88	-24.05	19:40:53.36	-32:52:20.0	0.156	0.159
Major+12	12.039	3.139	6.89	-26.15	19:50:29.47	-33:29:01.1	0.175	0.176
Minor-03	359.721	4.448	2.57	-14.47	18:51:13.29	-33:20:03.2	0.091	0.089
Minor-02	359.723	3.276	3.75	-14.21	18:52:14.06	-32:10:52.7	0.091	0.125
Minor-01	359.994	2.473	4.62	-14.29	18:54:09.13	-31:26:19.4	0.154	0.155
Minor+01	0.090	0.571	6.55	-13.94	18:56:06.96	-29:34:55.6	0.154	0.162
Minor+02	0.248	-0.610	7.77	-13.81	18:57:44.32	-28:26:40.7	0.202	0.206
Minor+03	0.181	-1.368	8.51	-13.56	18:58:00.68	-27:41:08.9	0.202	0.219
Minor+05	0.430	-3.494	10.69	-13.27	19:00:39.99	-25:37:45.8	0.224	0.204
SE+04	2.541	4.394	3.27	-17.20	19:04:34.06	-33:45:02.3	0.101	0.100
SE+02	1.206	2.916	4.46	-15.57	18:59:24.82	-32:04:48.7	0.121	0.118
NW+02	358.860	-0.122	6.94	-12.58	18:51:07.53	-28:41:03.5	0.177	0.173
NW+04	357.038	-1.359	7.81	-10.87	18:45:41.78	-27:11:49.2	0.148	0.265
SW+04	357.038	4.128	2.28	-11.79	18:39:00.43	-32:30:07.8	0.124	0.121
SW+02	358.607	2.686	4.08	-12.99	18:47:35.03	-31:23:49.9	0.123	0.153
NE+02	1.602	-0.003	7.50	-15.27	19:03:23.59	-29:15:40.7	0.157	0.118
ESE+07	5.341	4.836	3.46	-20.02	19:17:37.87	-34:34:38.3	0.095	0.095

^aThe Sgr coordinate system is described in Majewski et al. (2003) and is defined by virtue of the orientation of the extended tidal stream. However we note that (as shown in that same reference; see their Fig. 7) the main body of Sgr is canted by about 6° with respect to the mean orientation of the stream, so that our major and minor axis positions do not directly line up with the $(\Lambda_{\odot}, B_{\odot})$ system.

^b $\langle E(B - V) \rangle_{Phot}$ measured from Schlegel et al. (1998) for all 2MASS stars in the selection box for the field.

^c $\langle E(B - V) \rangle_{Spec}$ measured from Schlegel et al. (1998) for the spectroscopically measured Sgr members stars (see Table 2).

Table 2. Sagittarius Stellar Velocity Data

Field	NAME	$K_{s,o}$	$(J-K_s)_o$	E_{B-V}^a	l (deg)	b (deg)	Λ_{\odot} (deg)	V_{hel} (km s ⁻¹)	V_{GSR} (km s ⁻¹)	ϵ_V (km s ⁻¹)	TDR	Member?
Major+00	18541047–3026161	12.47	0.83	0.16	5.5688	–13.8964	359.824	+139.1	+168.2	2.2	15.91	Y
Major+00	18541810–3029314	12.11	0.98	0.15	5.5288	–13.9432	359.860	+146.8	+175.8	1.8	16.64	Y
Major+00	18543205–3047488	12.03	0.82	0.15	5.2612	–14.1105	359.962	–14.7	+13.2	2.6	11.15	N
Major+00	18550269–3045523	12.43	0.94	0.16	5.3367	–14.1983	0.065	+154.0	+182.2	1.8	20.41	Y
Major+00	18550257–3025397	12.60	0.75	0.15	5.6553	–14.0640	0.006	+144.4	+173.9	2.0	16.13	Y
Major+00	18542551–3039455	12.53	0.88	0.15	5.3785	–14.0356	359.916	+140.7	+169.1	2.3	18.08	Y
Major+00	18545211–3024229	12.67	0.79	0.15	5.6600	–14.0211	359.966	+139.2	+168.7	2.2	12.96	Y
Major+00	18542283–3051089	12.25	0.85	0.15	5.1951	–14.1023	359.940	+14.5	+42.2	2.7	14.92	N
Major+00	18553060–3047381	11.89	1.02	0.17	5.3498	–14.3017	0.168	+143.2	+171.5	1.9	24.95	Y
Major+00	18552942–3034507	10.58	1.12	0.15	5.5499	–14.2133	0.128	+134.5	+163.5	1.6	34.25	Y
Major+00	18553188–3041275	13.00	0.69	0.16	5.4491	–14.2651	0.155	+40.6	+69.2	1.7	10.74	N

^a $E(B - V)$ measured from Schlegel et al. (1998).

^bTable 2 is published in its entirety in the electronic edition of the *Astrophysical Journal*. A portion is shown here for guidance regarding its form and content.

Table 3. Field Kinematic Parameters

Field	$\langle V_{GSR} \rangle$ (km s ⁻¹)	$\sigma_{V_{GSR}}$ (km s ⁻¹)	R (′)	R_e (′)	RV stars
Major+00	170.14 ± 1.00	9.85 ± 0.73	10.7	23.1	102
Major-04	175.02 ± 2.09	15.60 ± 1.49	239.7	239.8	57
Major-02	172.91 ± 1.38	12.66 ± 0.98	110.9	112.0	86
Major+02	170.11 ± 1.01	13.39 ± 0.73	116.9	117.0	180
Major+04	167.93 ± 1.38	12.25 ± 1.00	234.0	234.3	82
Major+06	164.20 ± 1.55	11.44 ± 1.13	363.2	363.3	57
Major+08	165.19 ± 1.62	10.45 ± 1.18	486.5	486.6	44
Major+10	157.56 ± 2.97	14.34 ± 2.13	610.9	611.1	24
Major+12	152.15 ± 3.67	13.50 ± 2.62	740.2	740.2	14
Minor-03	167.40 ± 3.19	16.40 ± 2.27	179.2	511.7	27
Minor-02	173.58 ± 2.23	16.52 ± 1.58	109.2	311.1	56
Minor-01	173.33 ± 1.39	12.90 ± 1.00	59.7	170.1	89
Minor+01	172.73 ± 2.06	15.15 ± 1.48	54.7	156.2	56
Minor+02	167.46 ± 2.29	15.75 ± 1.64	126.1	360.0	48
Minor+03	156.28 ± 3.99	26.91 ± 2.83	171.0	488.5	46
Minor+05	154.54 ± 6.13	18.22 ± 4.36	299.0	854.4	9
SE+04	163.94 ± 2.51	14.44 ± 1.80	233.1	489.2	34
SE+02	171.20 ± 1.38	12.78 ± 0.99	112.8	242.1	88
NW+02	170.46 ± 1.66	12.90 ± 1.19	117.7	270.4	62
NW+04	175.95 ± 5.24	20.86 ± 3.75	229.7	486.1	16
SW+04	167.78 ± 2.62	8.19 ± 1.96	240.2	513.9	11
SW+02	174.51 ± 1.70	12.77 ± 1.24	111.0	236.7	60
NE+02	168.50 ± 2.53	15.03 ± 1.83	130.4	289.5	37
ESE+07	166.29 ± 2.70	13.34 ± 1.93	383.1	588.7	25
12°-15°	148.34 ± 2.79	9.05 ± 2.02	864	895	11
15°-20°	139.52 ± 3.95	11.67 ± 2.83	1045	1073	9
20°-40°	117.64 ± 4.92	16.93 ± 3.50	1675	1748	12
Ibata f1 AAT	155.45 ± 2.37	7.98 ± 1.60	718	638	15
Ibata f2 AAT	165.29 ± 3.18	11.03 ± 1.81	495	552	9
Ibata f3 AAT	168.95 ± 2.46	13.66 ± 2.19	455	409	17
Ibata f4 AAT	172.55 ± 1.92	11.96 ± 1.58	367	383	26
Ibata f5 AAT	172.15 ± 2.24	14.70 ± 2.12	56	69	30
Ibata f6 AAT	172.15 ± 2.33	14.70 ± 1.76	77	186	30
Ibata f7 AAT	169.05 ± 2.32	16.01 ± 1.62	32	36	44
Ibata f8 AAT	167.84 ± 3.30	18.70 ± 1.80			33
Ibata f1 CTIO	159.58 ± 2.06	10.80 ± 1.93	718	638	20
Ibata f5 CTIO	171.51 ± 1.22	9.24 ± 1.04	56	69	48
Ibata f6 CTIO	169.53 ± 2.76	13.29 ± 1.54	77	186	24
Ibata f7 CTIO	170.99 ± 0.80	11.41 ± 0.73	32	36	114
Bellazzini (Sgr,N)	168.03 ± 0.60	9.6 ± 0.4	0	0	318

Table 4. Expected Galactic Contamination

Field	Besaçon Stars Total	This Study Non-Members	Scale Factor	Expected Contaminants	This Study Members	Percent Contam.
Major+00	228	18	12.67	2.4 stars	102	2.4%
Major−04	573	57	10.05	9.8 stars	110	8.9%
Major−02	313	34	9.21	4.1 stars	86	4.8%
Major+02	210	34	6.18	2.6 stars	182	1.4%
Major+04	181	22	8.23	1.1 stars	82	1.3%
Major+06	150	29	5.17	2.7 stars	57	4.7%
Major+08	146	42	3.48	2.3 stars	45	5.1%
Major+10	120	55	2.18	1.8 stars	24	7.5%
Major+12	114	50	2.28	0.9 stars	14	6.4%
<i>Minor−03</i>	<i>247</i>	<i>91</i>	<i>2.71</i>	<i>25.8 stars</i>	<i>21</i>	<i>122.9%</i>
Minor−02	230	53	4.34	3.2 stars	56	5.7%
Minor−01	213	26	8.19	2.8 stars	89	3.1%
Minor+01	218	35	6.23	4.0 stars	56	7.1%
Minor+02	264	68	3.88	8.3 stars	48	17.3%
Minor+03	240	104	2.31	9.1 stars	49	18.6%
<i>Minor+05</i>	<i>244</i>	<i>78</i>	<i>3.13</i>	<i>10.2 stars</i>	<i>9</i>	<i>113.0%</i>
SW+04	354	29	12.21	2.0 stars	12	16.7%
SW+02	256	15	17.07	1.5 stars	60	2.5%
NE+02	203	12	16.92	1.1 stars	37	2.3%
<i>NW+04</i>	<i>369</i>	<i>60</i>	<i>6.15</i>	<i>10.7 stars</i>	<i>17</i>	<i>62.9%</i>
NW+02	270	49	5.51	8.5 stars	62	13.7%
SE+02	207	25	8.28	1.9 stars	88	2.2%
SE+04	198	45	4.40	4.6 stars	34	13.5%
ESE+07	156	66	2.36	3.8 stars	25	15.2%

Table 5. Supplementary Radial Velocity Data on M Giants Observed with the DuPont Telescope

NAME	$K_{s,o}$	$(J-K_s)_o$	$EB - V^a$	l (deg)	b (deg)	Λ_\odot (deg)	V_{hel} (km s ⁻¹)	V_{GSR} (km s ⁻¹)	CCP	Q	Member?
19531855 – 3448555	12.35	0.97	0.10	5.6	-27.1	12.7	126.1	151.3	0.50	7	Y
19534690 – 3459146	12.08	0.95	0.10	5.5	-27.2	12.8	124.6	149.3	0.45	6	Y
19541973 – 3525442	11.66	0.98	0.10	5.0	-27.4	12.9	142.8	165.7	0.44	7	Y
19544480 – 3431024	11.25	1.05	0.10	6.1	-27.3	13.0	115.7	142.5	0.74	7	Y
19553880 – 3547483	10.96	1.07	0.10	4.7	-27.8	13.2	135.3	157.0	0.71	7	Y
19571379 – 3359130	10.99	1.03	0.10	6.8	-27.6	13.5	114.2	143.3	0.69	7	Y
19572127 – 3626092	11.05	1.03	0.10	4.1	-28.3	13.6	132.3	151.9	0.81	7	Y
19591632 – 3411107	11.65	1.02	0.10	6.7	-28.1	13.9	-83.1	-54.5	0.27	4	N
20015401 – 3558348	9.76	1.18	0.10	4.9	-29.1	14.5	130.4	152.2	0.79	7	Y
20041192 – 3437541	10.85	1.07	0.10	6.5	-29.2	14.9	123.9	151.5	0.70	7	Y
20041677 – 3508590	10.27	1.14	0.10	5.9	-29.3	15.0	111.3	136.7	0.73	7	Y
20044613 – 3227255	10.68	1.08	0.10	8.9	-28.7	15.0	94.2	130.3	0.75	7	Y
20050480 – 3311517	10.47	1.13	0.10	8.1	-29.0	15.1	111.6	144.9	0.76	7	Y
20071791 – 3223480	12.39	0.93	0.20	9.2	-29.2	15.5	95.2	131.9	0.66	7	Y
20094440 – 3501218	10.90	1.08	0.10	6.4	-30.4	16.1	105.2	131.7	0.83	7	Y
20104667 – 3327077	10.67	1.09	0.10	8.2	-30.2	16.3	110.8	143.7	0.79	7	Y
20122492 – 3310058	10.96	1.06	0.20	8.6	-30.5	16.6	112.5	146.7	0.74	7	Y
20134595 – 3421279	10.96	1.06	0.10	7.4	-31.0	16.9	88.8	118.4	0.84	7	Y
20183323 – 3807468	11.45	0.99	0.10	3.2	-32.8	17.9	144.2	154.3	0.60	7	Y
20214447 – 3353414	11.04	1.04	0.10	8.3	-32.5	18.6	96.3	128.5	0.75	7	Y
20233705 – 3344500	11.36	1.08	0.10	8.6	-32.9	18.9	122.7	155.6	0.68	7	Y
20313337 – 3244528	11.48	1.04	0.10	10.2	-34.3	20.6	-29.2	8.1	0.82	7	N
20330508 – 3416310	10.53	1.13	0.00	8.5	-34.9	20.9	117.0	148.5	0.82	7	Y
20372047 – 3423140	11.44	1.03	0.00	8.5	-35.8	21.8	104.7	135.9	0.65	7	Y
20384078 – 3911581	11.15	1.00	0.00	2.7	-36.8	21.8	105.6	117.5	0.73	7	Y
20412659 – 3613296	11.49	1.00	0.00	6.5	-36.9	22.5	113.6	137.6	0.81	7	Y
20452019 – 3625220	11.16	0.99	0.10	6.4	-37.7	23.3	106.8	130.1	0.79	7	Y
20485427 – 3510562	10.87	1.07	0.10	8.1	-38.3	24.1	87.5	115.8	0.78	7	Y
20490681 – 3547523	11.35	1.01	0.10	7.3	-38.4	24.1	94.9	120.7	0.90	7	Y
20514595 – 3308115	10.59	1.14	0.10	10.8	-38.5	24.9	74.4	111.0	0.81	7	Y
21083956 – 3755451	10.46	1.11	0.00	5.1	-42.5	27.8	80.5	97.6	0.95	7	Y
21304974 – 3440522	10.53	1.11	0.10	10.1	-46.8	32.7	-1.4	27.3	0.76	7	N
21343307 – 3436437	10.12	1.24	0.00	10.3	-47.5	33.5	79.7	108.6	0.74	7	Y
21545225 – 3331355	10.81	1.11	0.00	12.3	-51.7	37.8	61.5	92.1	0.86	7	Y
22011809 – 3316344	11.31	0.98	0.00	12.8	-53.0	39.2	65.6	96.3	0.88	7	Y
22263275 – 3404084	11.56	1.03	0.00	11.3	-58.2	44.1	-133.2	-110.4	0.70	7	N
22514994 – 3659556	11.06	1.08	0.00	4.0	-62.9	48.2	-126.0	-120.7	0.92	7	N

^a $E(B - V)$ measured from Schlegel et al. (1998).

Table 6. Properties of the Classical Milky Way dSph Galaxies

Name	Distance (kpc)	L_V^b ($L_{V,\odot}$)	r_{half}^b (pc)	ϵ^c	$\sigma_{V,central}$ (kms^{-1})	$M(r_{half})^b$ (M_\odot)
Leo II	219	5.9×10^5	151	0.13	6.6 ± 0.7	3.8×10^6
Carina	72	2.4×10^5	241	0.33	6.6 ± 1.2	6.1×10^6
Sextans	95	4.1×10^5	682	0.35	7.7 ± 1.3	2.5×10^7
Draco	69	2.7×10^5	196	0.29	9.1 ± 1.2	9.4×10^6
Leo I	254	3.4×10^6	246	0.21	9.2 ± 1.4	1.2×10^7
Sculptor	85	1.4×10^6	260	0.32	9.2 ± 1.1	1.3×10^7
Ursa Minor	93	2.0×10^5	280	0.56	9.5 ± 1.2	1.5×10^7
Sagittarius	29	1.7×10^7	1550	0.65	9.9 ± 0.7	1.2×10^8
Fornax	139	1.4×10^7	668	0.30	11.7 ± 0.9	5.3×10^7

^aReferences: Distances adopted from Rizzi et al. (2007) for Fornax, Bellazzini et al. (2004) for Leo I, Pietrzyński et al. (2008) for Sculptor, Siegel & Majewski (2006) for Leo II, Lee et al. (2003) for Sextans, Bellazzini et al. (2002) for Draco, Mighell & Burke (1999) for Ursa Minor and Siegel et al. (2011) for Sagittarius.

^bValues taken from Walker et al. (2010), see original paper for references therein

^cReferences: Ellipticity adopted from Irwin & Hatzidimitriou (1995) for Sextans, Fornax, and Leo II Sohn et al. (2007) for Leo I, Westfall et al. (2006) for Sculptor, Odenkirchen et al. (2001) for Draco, Palma et al. (2003) for Ursa Minor, and PAPER I for Sagittarius.

^dReferences: Central Velocity Dispersion adopted from Walker et al. (2009) for Fornax, and Sextans, Sohn et al. (2007) for Leo I, Westfall et al. (2006) for Sculptor, Mateo et al. (2008) for Leo II, Odenkirchen et al. (2001) for Draco, Palma et al. (2003) for Ursa Minor, and This paper for Sagittarius.

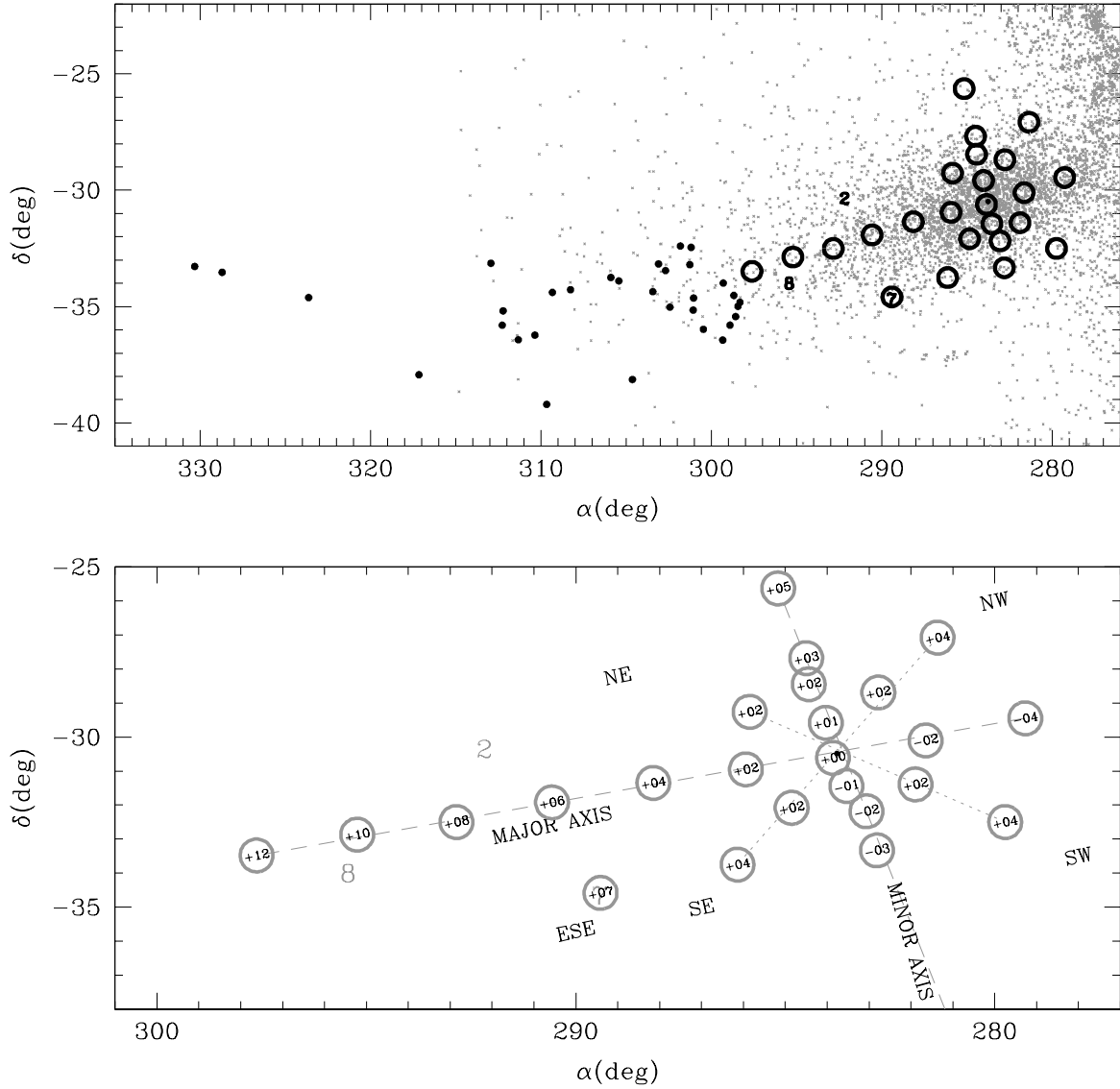


Fig. 1.— (a) View of the central parts of Sgr and the location of our survey fields. M giants from PAPER I up to $b = -5^\circ$ are shown. The locations of globular clusters are marked as follows: “2” is Arp 2, “7” is Terzan 7, “8” is Terzan 8. Black points are the locations of the additional stars described in §5.1 (b) Same as shown in (a) but with fields identified with descriptive labels.

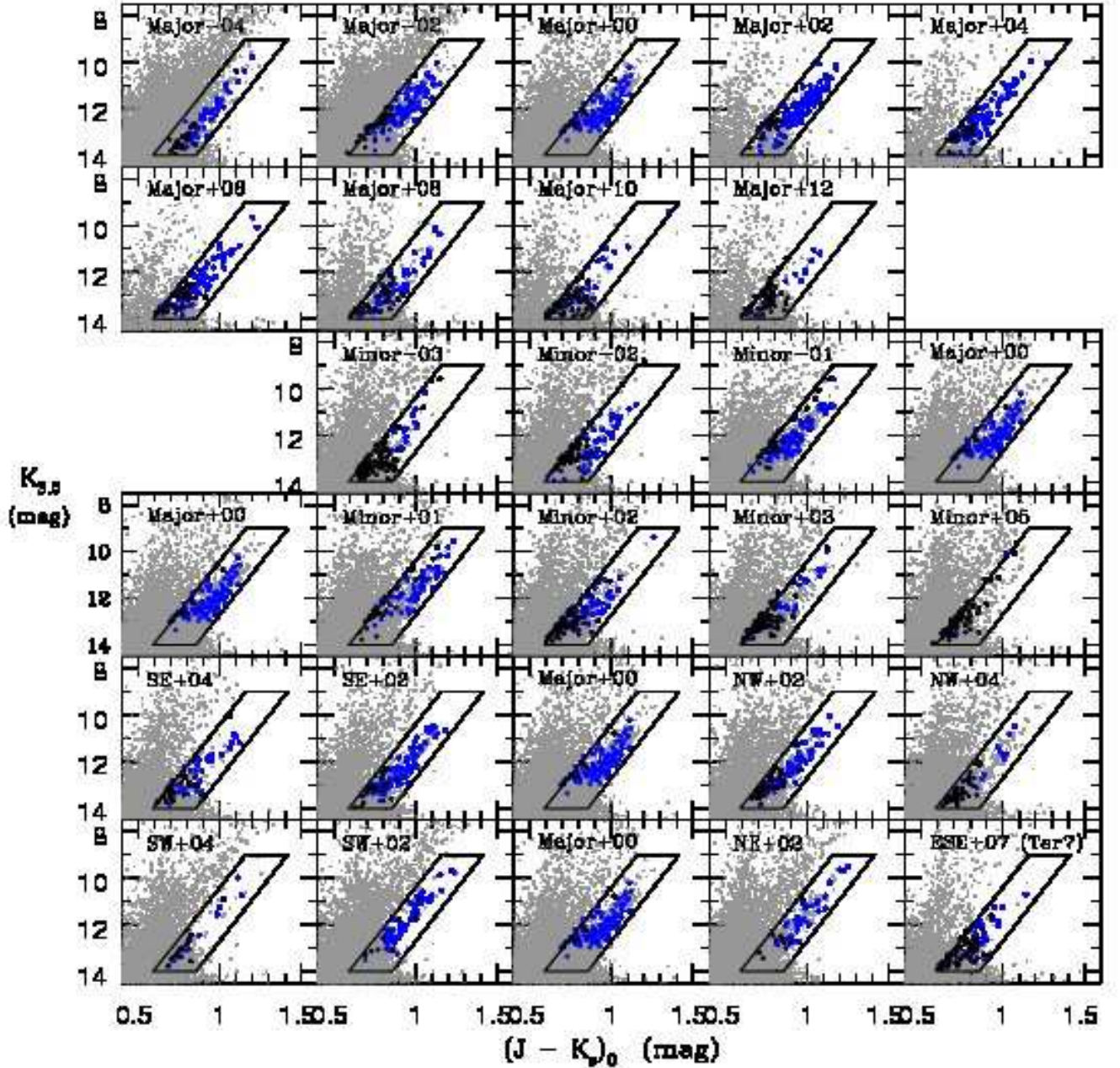


Fig. 2.— Dereddened 2MASS color-magnitude diagrams for each observed field. The box delimits the selection criterion used to select Sgr RGB candidates for targeting. Sgr member stars based on the RV as described in §3 are shown in black, non-members are shown in blue. The panel corresponding to the center field (i.e., “Major+00”) appears several times in the figure to complete sequences of panels corresponding to different cross-sections across the Sgr system. (Degraded image for astro-ph)

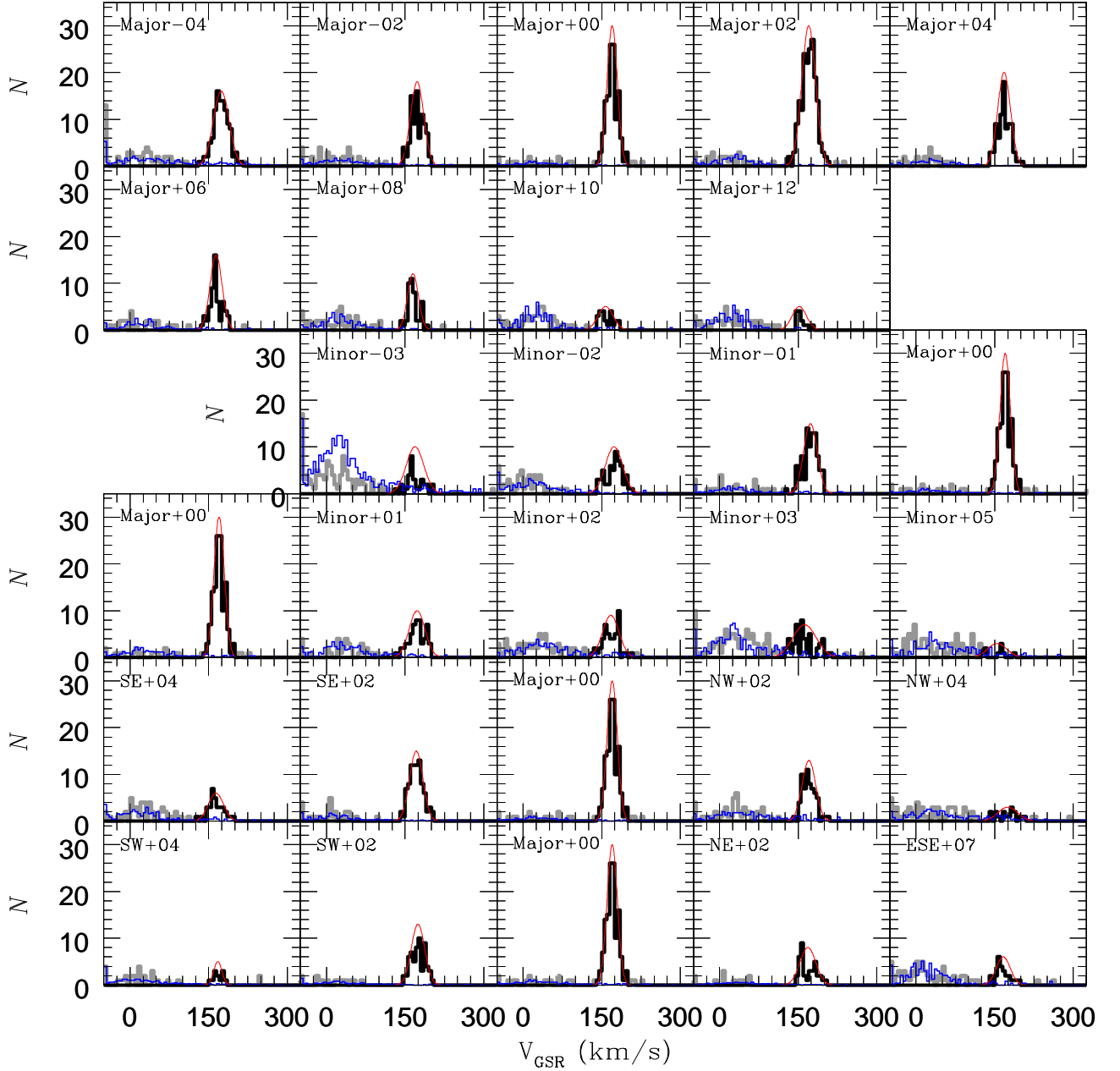


Fig. 3.— Radial velocity distributions for each field pointing (grey histograms). The lowest probability Sgr members were selected against using a 3σ , iterative rejection scheme. The black histogram shows the stars within 3σ of the Sgr mean value. The measured means and dispersions of the selected members are shown as Gaussians (red line), based on data from Table 3. The blue lines show the results of the Besançon Galaxy Model (Robin et al. 2003) for these fields scaled to the number of non-members, and showing the generally low level of contamination.

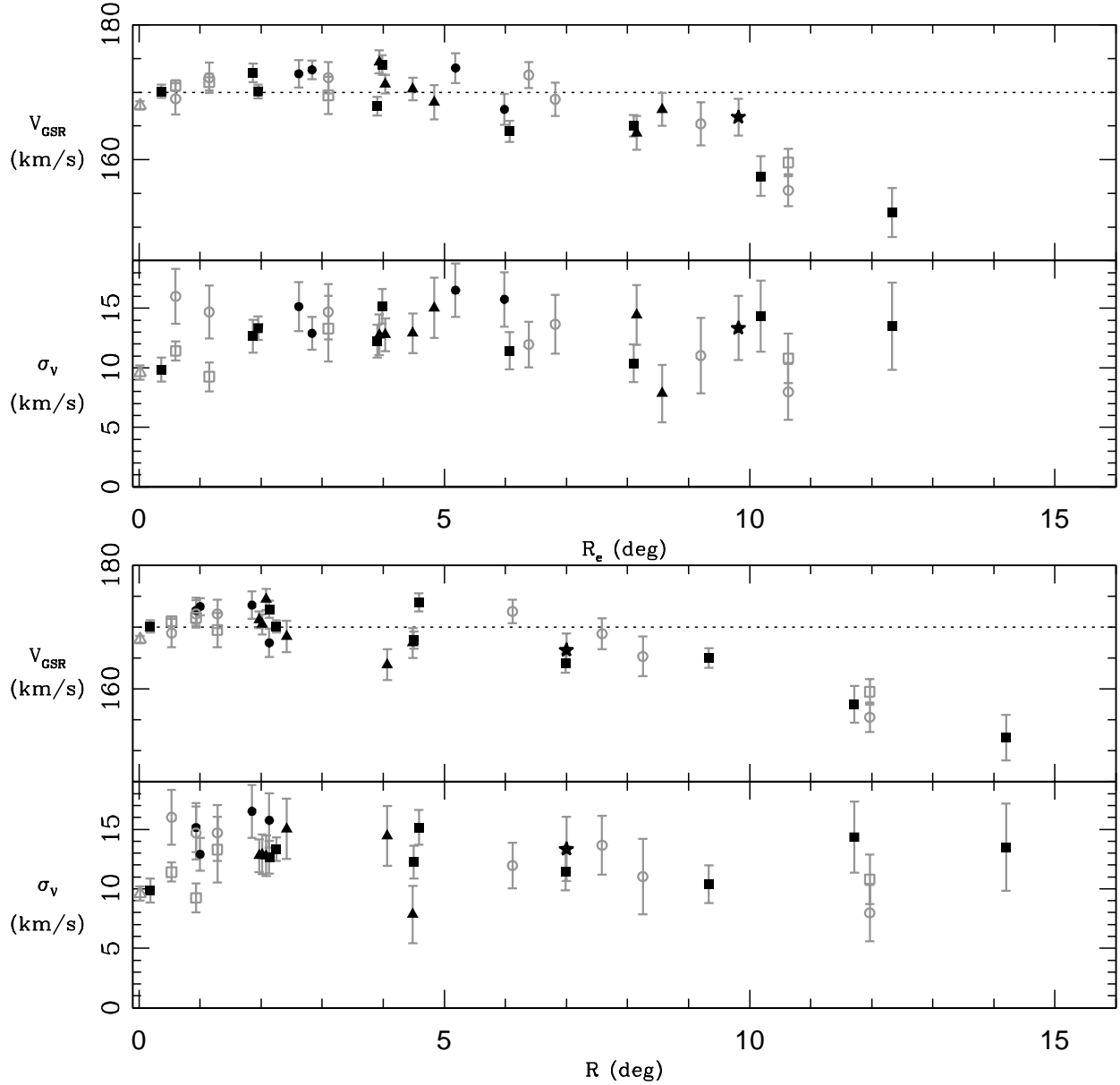


Fig. 4.— Velocity and velocity dispersion trends as a function of projected circular (R) and elliptical (R_e) radii. Black squares denote fields on the major axis, black circles the minor axis, black triangles are from the diagonal fields (NW, SW, NE, SE), and the black star is the ESE+07 or Ter7 field. The fields from Ibata et al. are included as grey open circles for the AAT fields and open squares for the CTIO fields. The Bellazzini et al. field (Sgr,N) is shown as an open triangle.

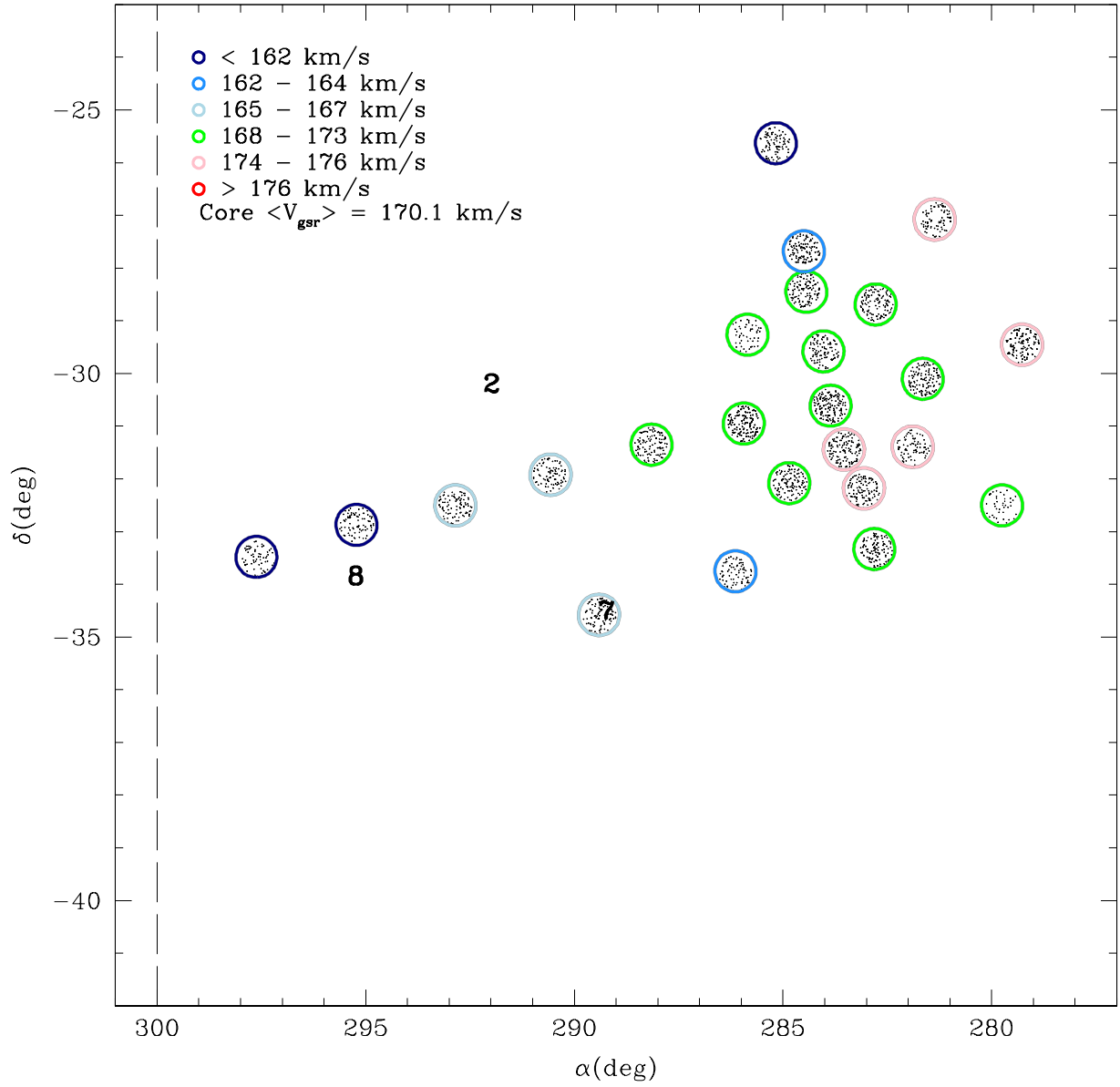


Fig. 5.— View of the central parts of the Sgr core showing the general trends of mean V_{GSR} .

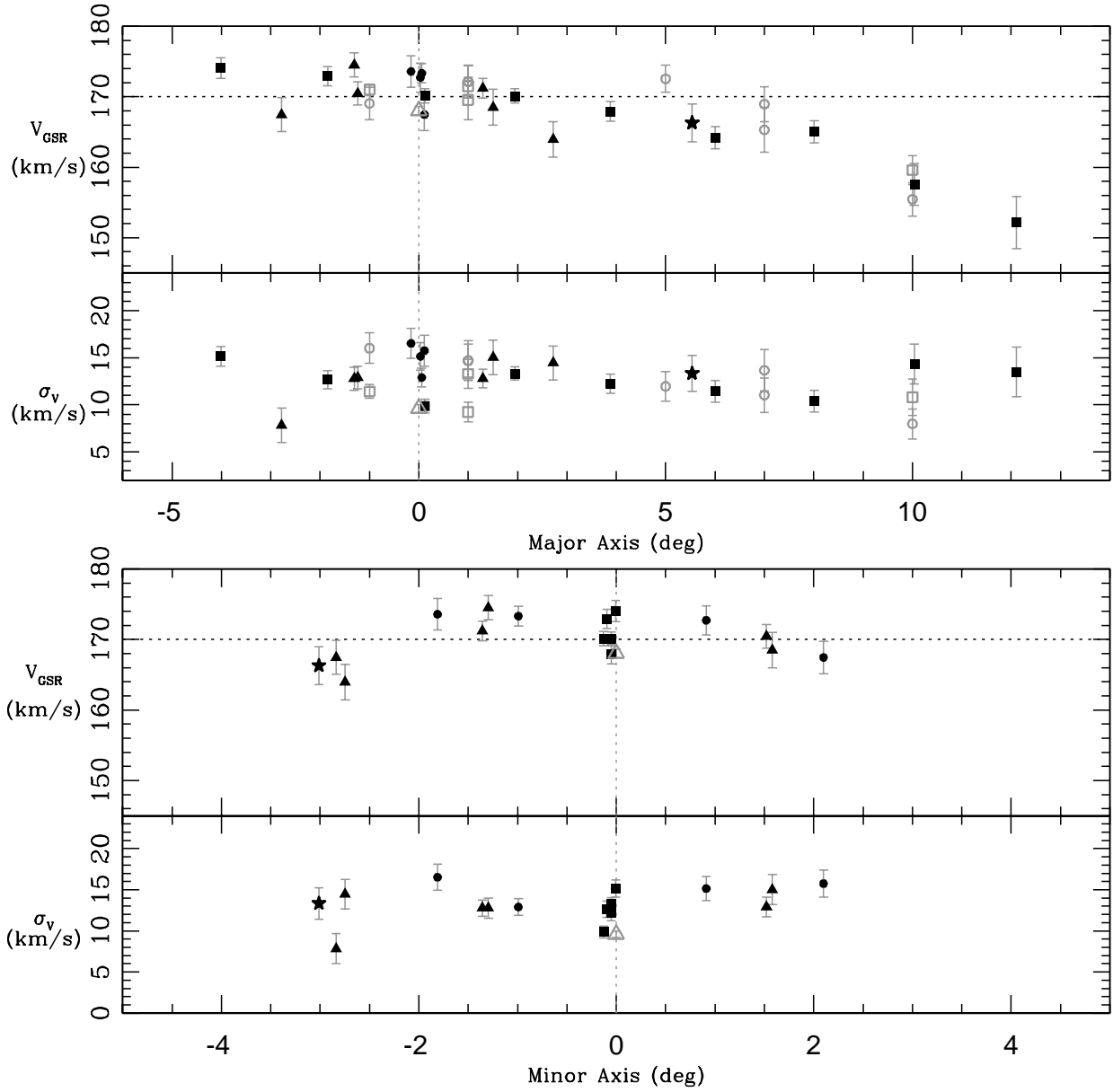


Fig. 6.— Velocity and velocity dispersion as a function of major axis and minor axis position. Symbols are same as Figure 4.

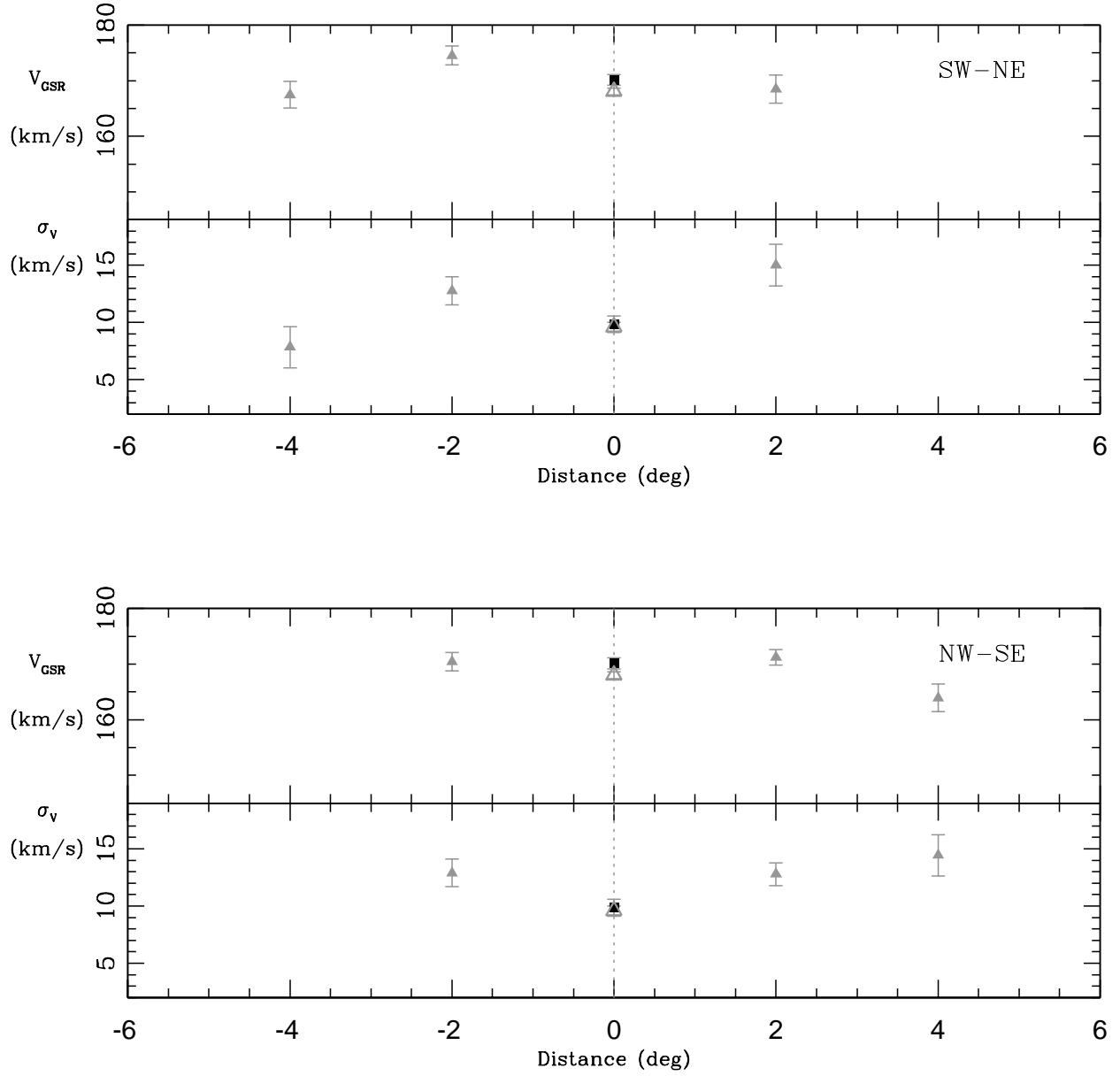


Fig. 7.— Velocity and velocity dispersion trends along the diagonal axes from SW+04 across the core to NE+02 (upper two panels) and from NW+04 across the core to SE+04 (lower two panels). Symbols and colors are same as Figure 4.

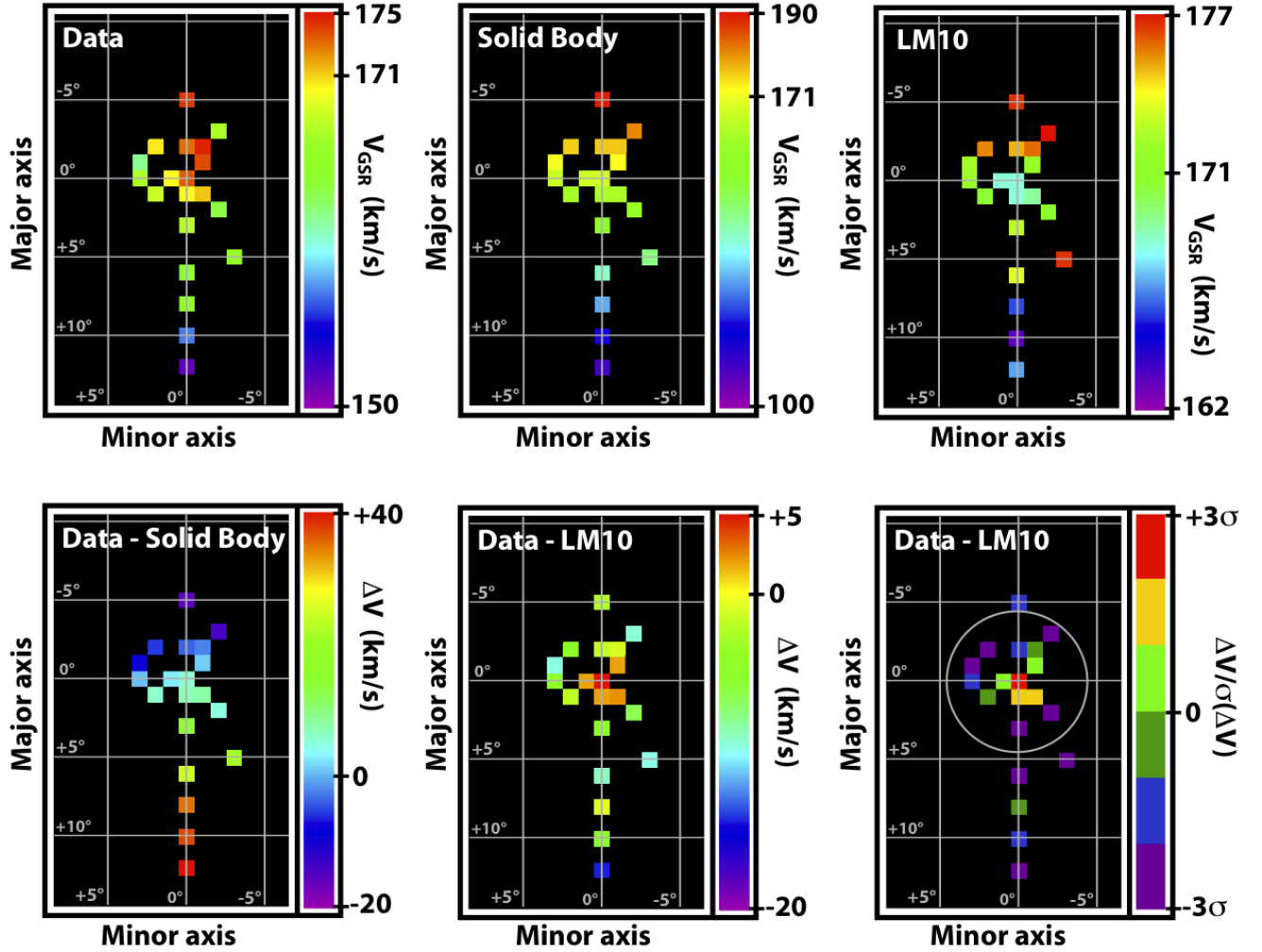


Fig. 8.— Top row: Velocity maps for the observational data, a solid-body model moving with the space velocity of Sgr determined by LM10, and the N -body model of LM10. Sampling of the models is chosen to match the observational data. Bottom row: Residual velocity difference between the observational data and the solid-body and N -body models. The bottom right panel shows the significance of positive/negative residuals between the observational data and the N -body model. The grey circle in the bottom right panel indicates the $\sim 4.5^\circ$ radius at which unbound stars are expected to constitute $\sim 50\%$ of the stars in a given field based on the LM10 model.

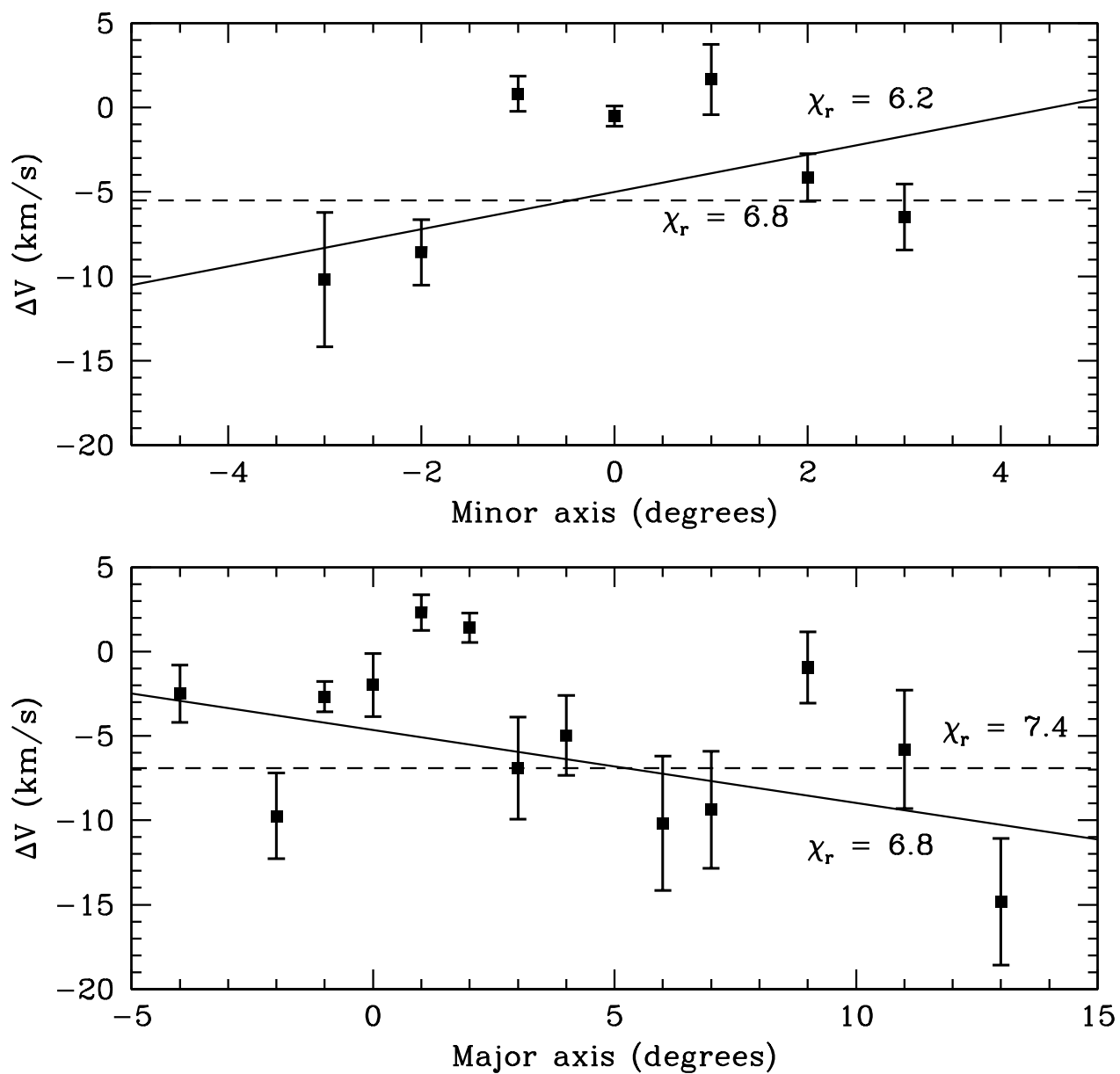


Fig. 9.— Linear least-squares fits to the velocity residuals (observational data minus LM10 N -body model) along the major (bottom panel) and minor (top panel) axes. Values for the square root of reduced χ^2 for each fit are shown.

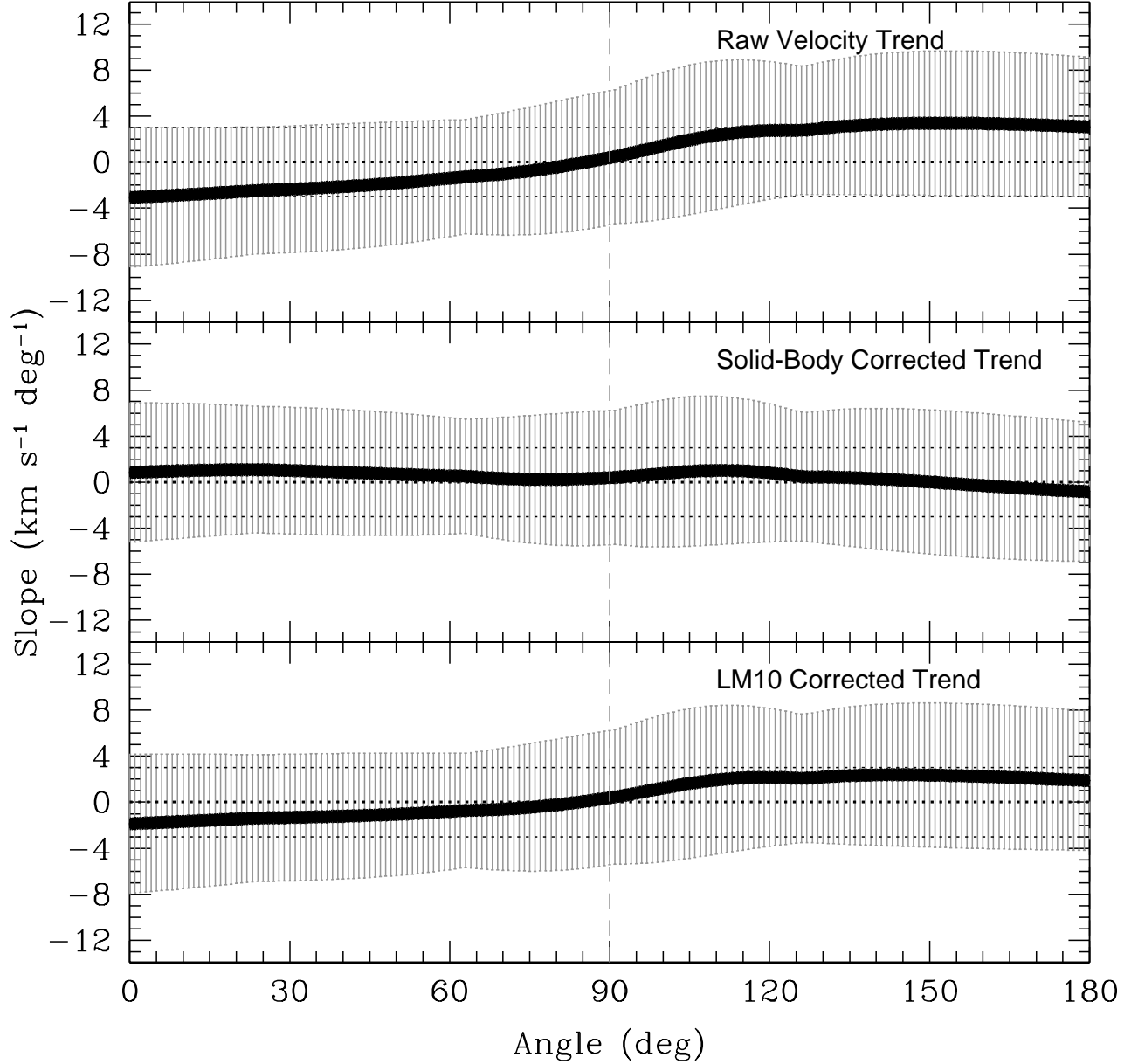


Fig. 10.— To test for various effects of galaxy rotation, we projected all stars along the major axis (Angle - 0) and determined the slope (black points) and dispersion (grey bars). We then repeated these projection on axes in 1° increments through 180° (back to the Major Axis). Minor axis is denoted by the dashed line at 90° (a) Observed trend with no corrections. (b) Observed trend corrected by including the effects of solid-body orbital motion. (c) Observed trend corrected by including the modeled dynamical effects from Law & Majewski (2010) model for the global trends of Sgr.

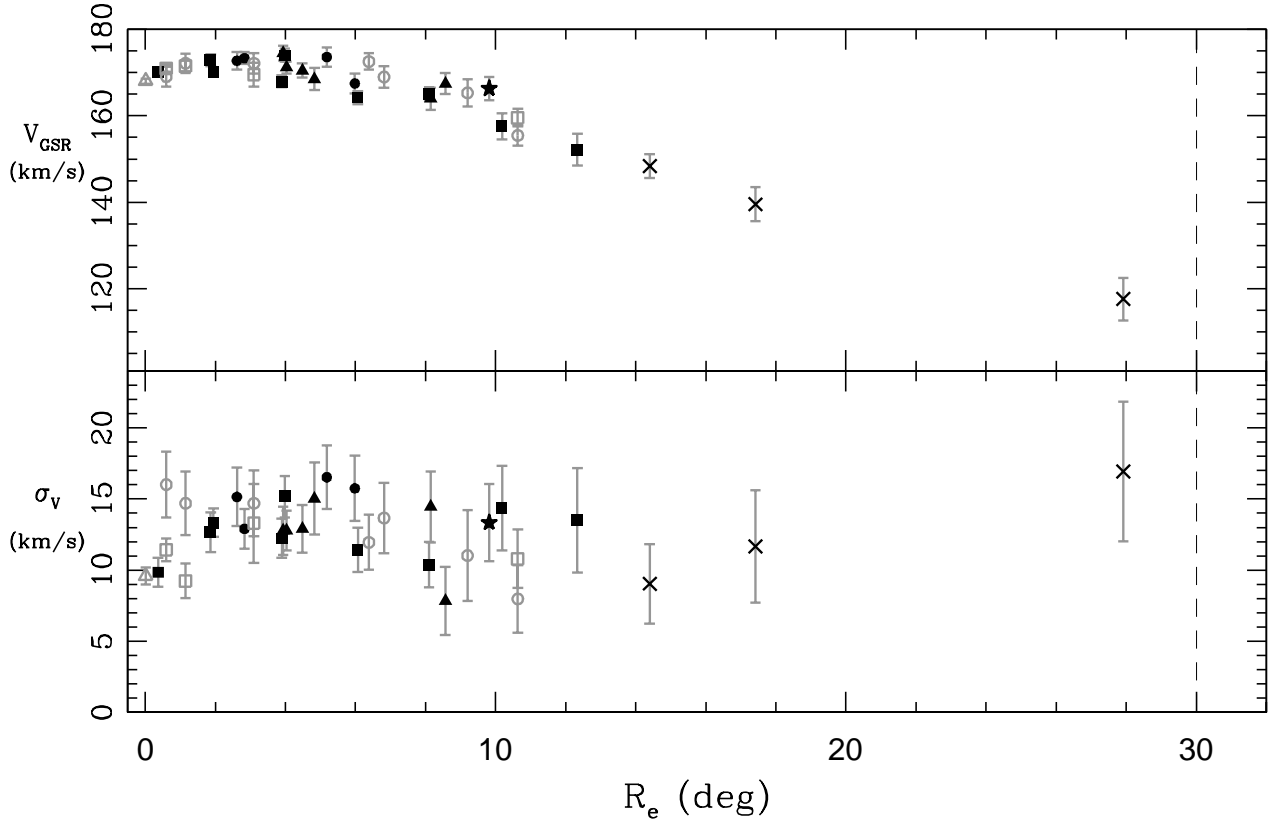


Fig. 11.— Velocity and velocity dispersion trends as a function of projected elliptical (R_e) radii, including supplemental data from §5.1. The new measurements are shown as black crosses, and the King limiting radius derived in PAPER I is shown as a dashed line at $\sim 30^\circ$. As in Figure 4, black squares denote fields on the major axis, black circles the minor axis, black triangles are from the diagonal fields (NW, SW, NE, SE), and the black star is the ESE+07 or Ter7 field. The fields from Ibata et al. are included as grey open circles for the AAT fields and open squares for the CTIO fields. The Bellazzini et al. field (Sgr,N) is shown as an open triangle.

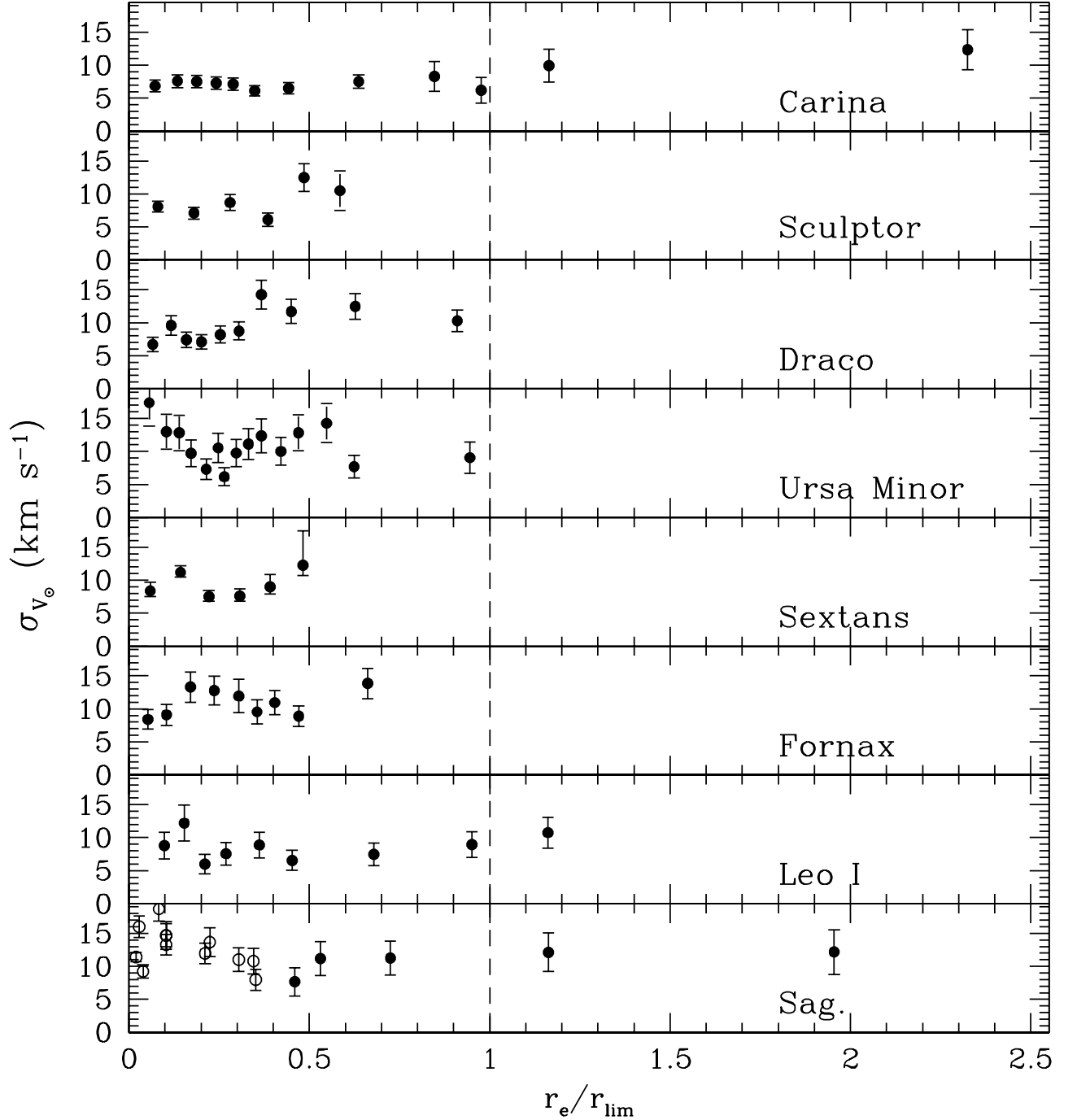


Fig. 12.— Observed trend of velocity dispersion profiles versus projected radius for Milky Way dSphs. The vertical line designates the King limiting radii for the different objects, to which the abscissa has been scaled. Similar profiles have been reported by other authors (e.g., Walker et al. 2007). REFERENCES: Carina (Muñoz et al. 2006), Sculptor (Westfall et al. 2006), Draco and Ursa Minor (Muñoz et al. 2005), Sextans (Walker et al. 2009), Leo I (Sohn et al. 2007), Sagittarius (This paper, Majewski et al. 2004)

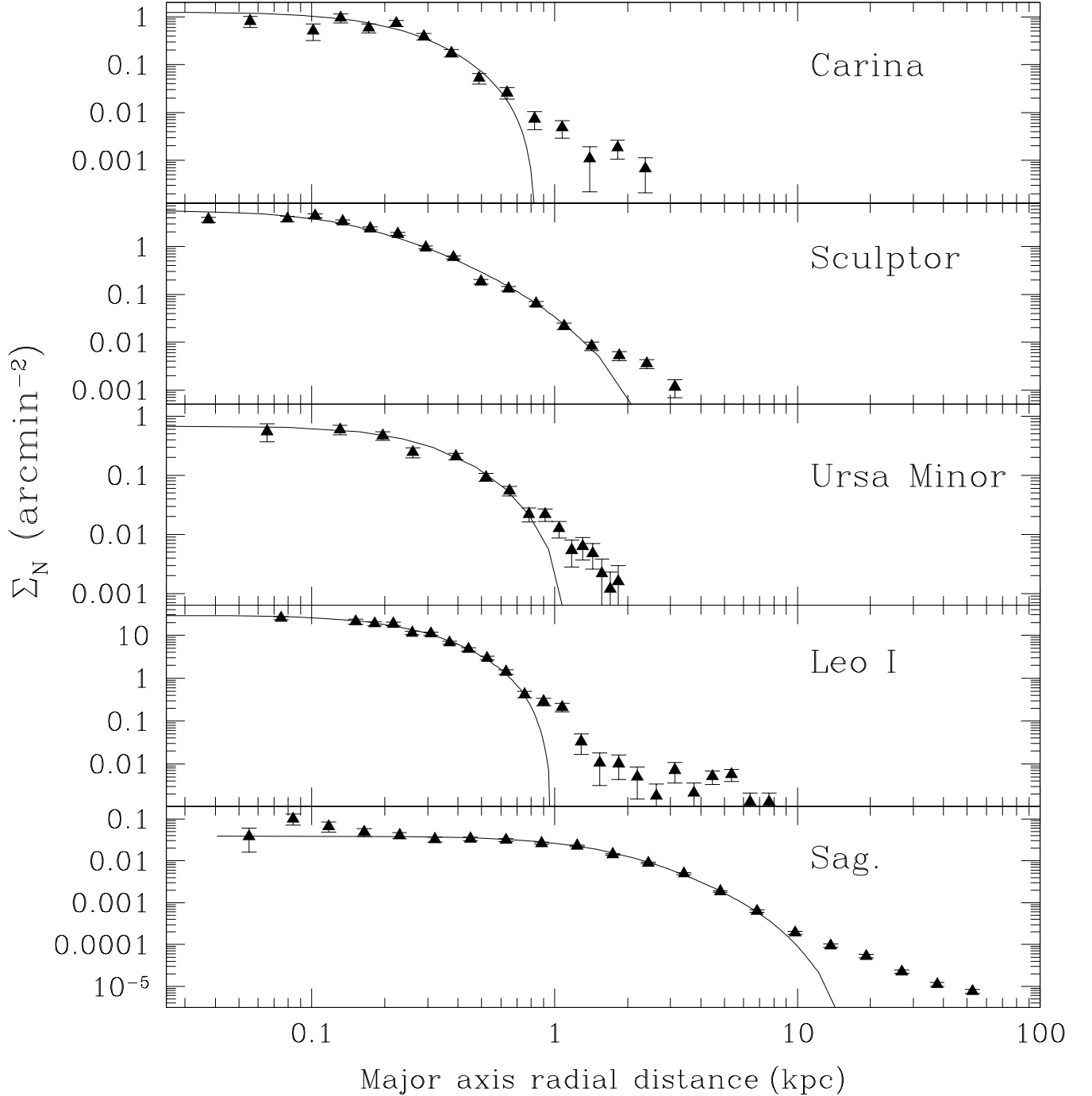


Fig. 13.— Radial number density profiles of associated red-giant-branch candidates (minus the mean field giant background) for five dSphs. The solid lines show King profiles fit to the central regions. Error bars represent Poisson errors. REFERENCES: Carina (Muñoz et al. 2006), Sculptor (Westfall et al. 2006), Ursa Minor (Palma et al. 2003), Leo I (Sohn et al. 2007), Sagittarius (Majewski et al. 2003)